sciendo
Austrian Journal of Earth Sciences | Vienna | 2025 | Volume 118 | 75–94 | DOI: 10.17738/ajes.2025.0004

Diabase is petrologists best friend: quantitative *P-T* constraints on the NW-SE trending Eoalpine metamorphic gradient in the western Austroalpine nappe stack (Ötztal Nappe, Texel Nappe, Silvretta Nappe) using metamorphosed mafic dikes

Gabriel Raso[1*], Peter Tropper[1], Hannah Pomella[2], Dieter Rammlmair[3]

[1)] Institute of Mineralogy and Petrography, University of Innsbruck, 6020 Innsbruck, Austria
[2)] Institute of Geology, University of Innsbruck, 6020 Innsbruck, Austria
[3)] Institute of Mineralogy, Leibniz University, Hannover, Germany
[*)] Corresponding author: Gabriel Raso, email: gabriel.raso@uibk.ac.at

Keywords: metamorphic mafic dikes, Ötztal Nappe, Eoalpine metamorphism, geothermobarometry, metamorphic petrology

Abstract

The Ötztal Nappe (Austroalpine Superunit, Eastern Alps) is volumetrically the largest polymetamorphic nappe of the western Austroalpine nappe stack and consists of paragneisses and micaschists with various intercalations of orthogneisses, amphibolites and rare marbles. The main foliation of these rocks is cross-cut by numerous dikes of basaltic to andesitic composition. Field- and textural investigations reveal that these dikes underwent only Eoalpine metamorphism and deformation and are not part of the earlier Variscan history of the region. While quantitative Eoalpine *P-T* data are only available from the central and southeastern Ötztal Nappe, almost no such data is available from the northwestern part of the nappe. The aim of this study therefore is to refine the *P-T* constraints of the northwest to southeast trending Eoalpine metamorphic gradient in the western Austroalpine nappe stack especially in the central and northwestern Ötztal Nappe using metamorphic mafic dikes. For this purpose, multi-equilibrium geothermobarometry paired with classical geothermobarometry was performed on 19 dike samples from the Ötztal Nappe, the Texel Nappe and the Silvretta Nappe from the investigations of Rammlmair (1980). The metamorphic mafic dikes contain the mineral assemblage plagioclase + amphibole + quartz + chlorite + epidote + titanite ± biotite ± muscovite ± garnet. The anorthite content in plagioclase and the tschermakite and edenite component in Ca-amphiboles are clear mineral chemical indicators for increasing *P-T* conditions from the northwest to the southeast of the Ötztal Nappe. The thermobarometric calculations with multi-equilibrium geothermobarometry (THERMOCALC v.3.21) yield *P-T* conditions of 250–300 °C and 2–4 kbar for the northwestern Ötztal Nappe, reaching 550–600 °C and 8–10 kbar in the southeastern Ötztal Nappe, adjacent to the Schneeberg Nappe. The metamorphic mafic dike from the western Texel Nappe yields *P-T* conditions of 540±41 °C and 8.9±1.6 kbar. Geothermobarometric calculations using THERMOCALC v.3.45 yield similar results. Our results represent the first quantitative *P-T* estimates of the complete northwest to southeast trending Eoalpine metamorphic field gradient in the Ötztal Nappe above and below the chloritoid isograd.

1. Introduction

The Ötztal Nappe (ÖN) is a large, polymetamorphic nappe, which is part of the western Austroalpine nappe stack in the European Eastern Alps (Fig. 1). It consists mainly of paragneisses and micaschists with various intercalations of orthogneisses, amphibolites and rare marbles. The main foliation of these rocks is cross-cut by numerous dikes of basaltic to andesitic composition. Field- and textural investigations reveal that these dikes underwent only Eoalpine metamorphism and deformation and are not part of the Variscan earlier history of the region (Ampferer and Hammer, 1924; Hammer, 1929; Harre et al., 1968).

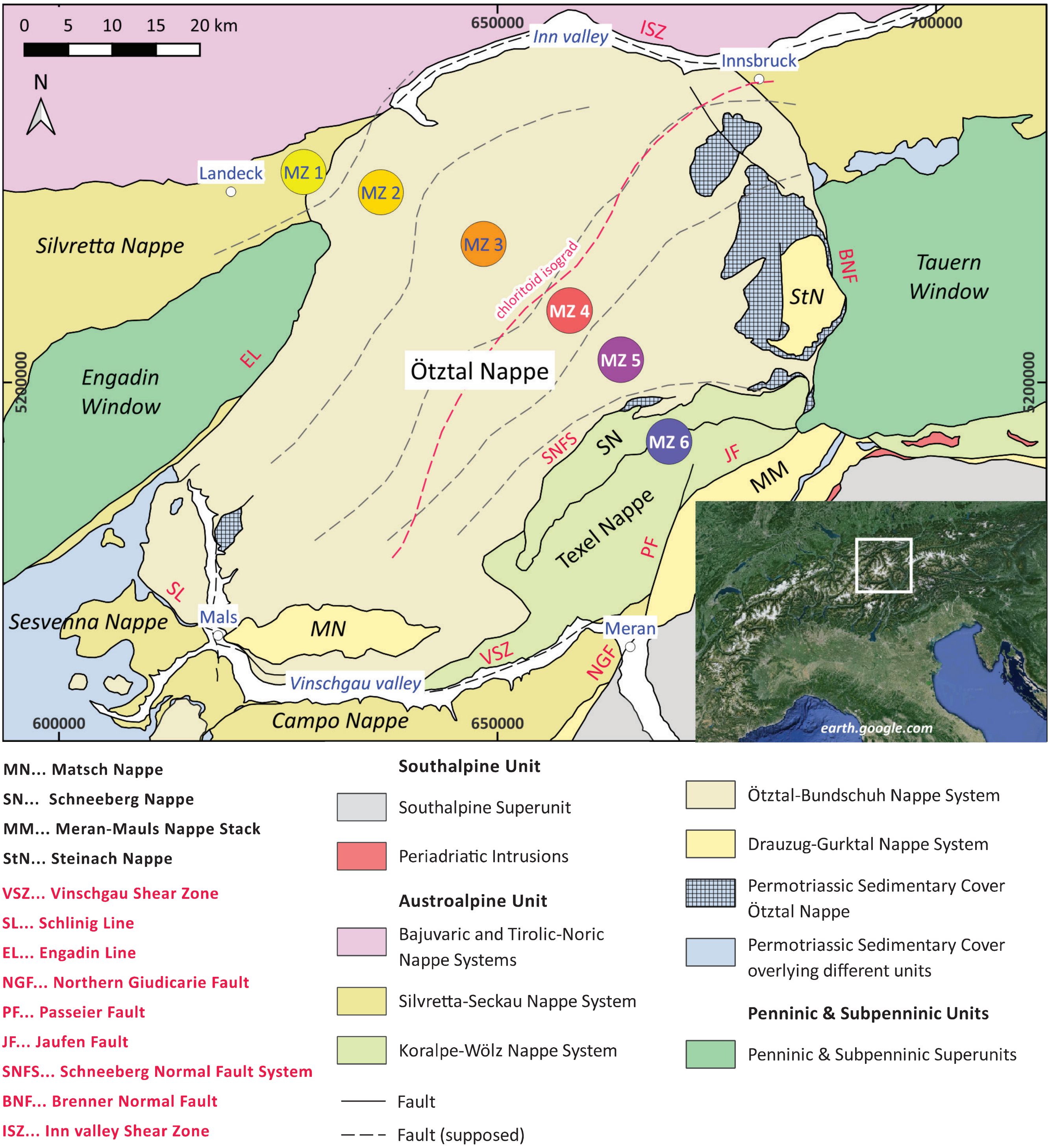

Figure 1: Tectonic map of the investigated area (modified from https://geokatalog.buergernetz.bz.it). The six metamorphic zones after Purtscheller and Rammlmair (1982) are represented by coloured spheres and delimited by grey dashed lines. The Eoalpine chloritoid isograd after Purtscheller (1967) is represented by a red dashed line.

Metamorphic mafic dikes from the ÖN have been used to indicate qualitatively the increase of the Eoalpine metamorphic overprint from northwest to southeast of the ÖN (Purtscheller and Rammlmair, 1982). Quantitative *P-T* data concerning the Eoalpine metamorphic gradient have only been determined for the southeastern ÖN and the adjacent tectonic units, the Schneeberg- and the Texel Nappe (Hoinkes, 1981; Tessadri, 1981; Dietrich, 1983; Hoinkes et al., 1991; Spalla, 1993; Konzett and Hoinkes, 1996; Sölva et al., 2001; Tropper and Recheis, 2003; Habler et al., 2006; Tribus et al., 2008; Zanchetta et al., 2013; Miladinova et al., 2022; Tropper et al., 2023). So far, no quantitative *P-T* data concerning the Eoalpine metamorphic gradient for the central and northwestern ÖN are available.

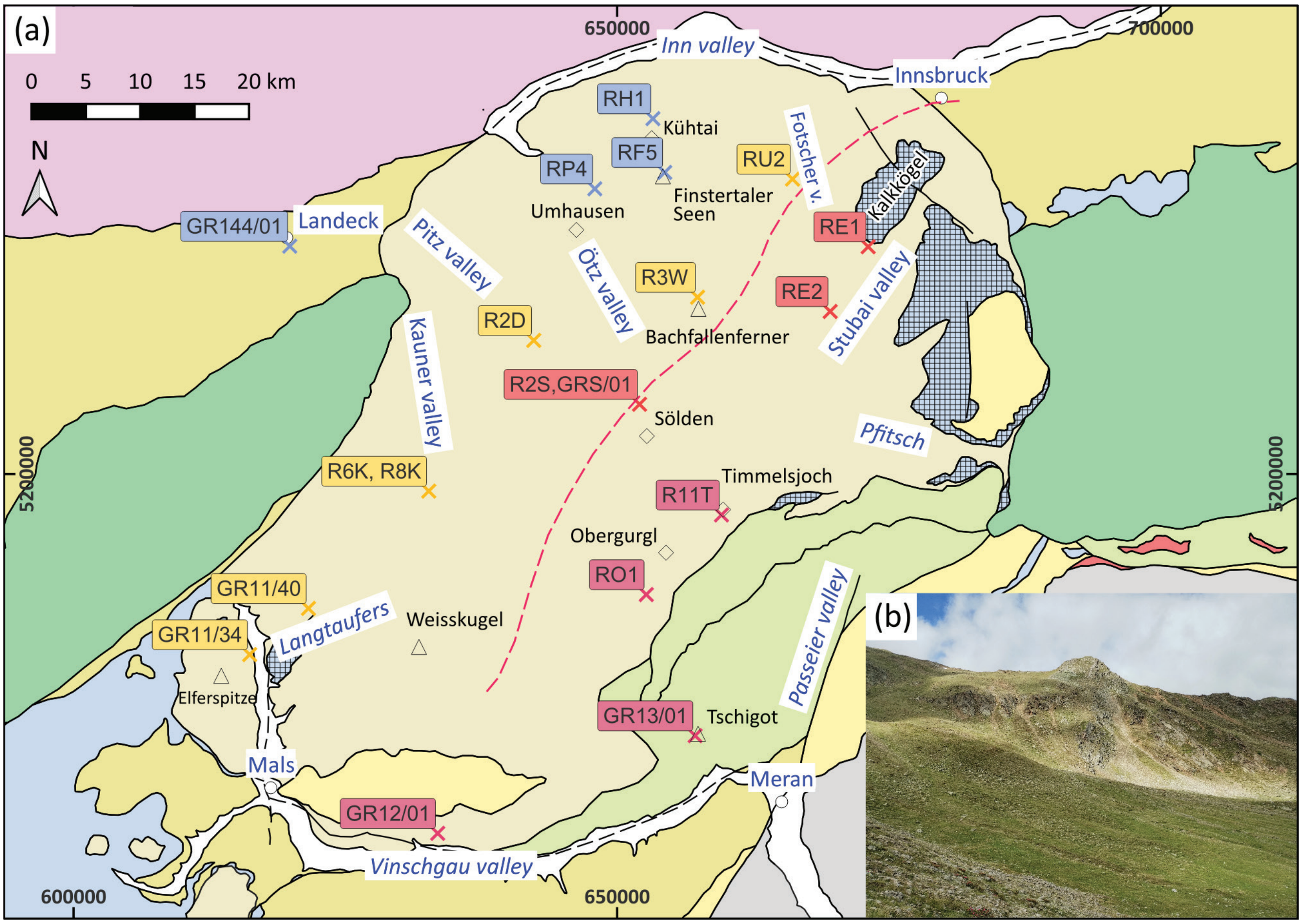

Figure 2: (a) Sample localities of the investigated dikes. The samples are coloured with respect to their mineral assemblage and metamorphic zone after Purtscheller and Rammlmair (1982) as discussed in section 3. The tectonic units are the same as in Figure 1, the red dashed line represents the Eoalpine chloritoid isograd after Purtscheller (1967). **(b)** Field overview of a metamorphosed mafic dike (GR11/34).

The aim of this study is to extend the quantitative *P-T* constraints of the Eoalpine metamorphic gradient in the northwestern and central part of the ÖN by using these monometamorphic mafic dikes. In fact, the Eoalpine metamorphic gradient can best be studied on these dikes because they are of the same lithology across the entire gradient and for that reason the gradient is of extremely high tectonic interest. Therefore, the mineral chemistry of 17 dike samples from the ÖN, based on samples from Rammlmair (1980), were analysed and multi-equilibrium geothermobarometry paired with classical geothermobarometry was performed. Additionally, one dike sample from the Silvretta Nappe (SN) in the northwest and one from the Texel Nappe (TN) in the southeast were analysed to see if there is an Eoalpine prograde *P-T* correlation between the three adjacent tectonic units.

1.1. Geological setting and metamorphism

The ÖN is located between the Inn valley in the north (North Tyrol, Austria) and the Vinschgau in the south (western South Tyrol, Italy). This Austroalpine nappe extends between two tectonic windows (Fig. 1): In the west, the Engadin Line represents the boundary between the ÖN and the Engadin window (Schmid and Froitzheim, 1993), in the east the ÖN is offset from the Tauern window along the Brenner Normal Fault (Behrmann, 1988; Selverstone, 1988). In the north, the dextral Inn valley shear zone represents the boundary between the ÖN and the Northern Calcareous Alps (Ortner et al., 2006). In the northwest the ÖN borders to the Landeck Quartzphyllite and the Phyllite Gneiss Zone, which corresponds to the northern part of the Silvretta Nappe (Maggetti and Flisch, 1993). In the south the ÖN is separated from the Sesvenna Nappe, the Campo Nappe and the Texel Nappe along the sinistral Vinschgau Shear Zone (VSZ; Montemagni et al., 2023) and its western continuation, the Schlinig Line (Schmid and Haas, 1989; Fig. 1). The VSZ branches out towards the east, where the northern branch extends into the Schneeberg Normal Fault System (SNFS; Sölva et al., 2005), which separates the ÖN from the Texel Nappe. The Matsch Nappe is situated in a hanging wall position with respect to the VSZ (Habler et al., 2009). It's origin and tectonometamorphic attribution to the Austroalpine nappe stack is still under discussion (Pomella et al., 2022).

The ÖN is a polymetamorphic nappe that is cross-cut by numerous dikes of basaltic to andesitic composition (Purtscheller and Rammlmair, 1982). These dikes are striking mostly northeast-southwest, but also north-south and northwest-southeast striking dikes occur. Their thickness varies between 0.5 and 30 m. They can be traced along strike for several hundreds of meters. The crystalline basement of the ÖN is covered by a Permomesozoic (meta-)sedimentary succession. This is the so-called "Brennermesozoikum" (BM; Kübler and Müller, 1962), which is exposed in the eastern parts of the ÖN, and which contains no metamorphosed mafic dikes thus providing a pre-Mesozoic age limit to the dikes.

The crystalline basement of the ÖN underwent at least three metamorphic overprints: The oldest is Ordovician in age (490–460 Ma), leading to the formation of orthogneisses and scattered occurrences of migmatites (e.g., Thöny et al., 2008). The second was the Variscan event, with a first stage of high-pressure metamorphism, leading to the formation of eclogites in the central and western parts of the ÖN (Miller and Thöni, 1995). The second and more dominant Variscan amphibolite-facies stage of metamorphism reached 570–640 °C and 5.8–7.5 kbar in the northwestern ÖN around 340–330 Ma (Tropper and Hoinkes, 1996). The third and most recent metamorphic overprint occurred in the Cretaceous during the Eoalpine Orogeny (100–73 Ma; Thöni, 1999). Metamorphic assemblages formed during Eoalpine metamorphism vary within the ÖN, from lower greenschist-facies in the northwest to epidote-amphibolite facies in the southeast. This was already constrained by Thöni (1980) in the ÖN using K-Ar and Rb-Sr data of white mica and biotite which show a striking rejuvenation of mica ages from Variscan in the northwest to Eoalpine in the southeast. Purtscheller and Rammlmair (1982) constrained the Eoalpine metamorphic conditions in the ÖN based on six metamorphic mineral zones (MZ, Fig. 1) and the mineral chemistry of the post-Variscan metamorphosed mafic dikes. This is well established by the chemical variability of hornblende and by the anorthite content of plagioclase from the metamorphic mineral assemblage. In the southeastern ÖN the *P-T* conditions range from 550 to 600 °C and 7.2 to 8.8 kbar (Tropper and Recheis, 2003), with the metamorphic peak at ~88 Ma (Harre et al., 1968). In the Schneeberg Nappe *P-T* conditions of 550 to 600 °C and 8 to 10 kbar at ~93–91 Ma were estimated (Hoinkes, 1981; Konzett and Hoinkes, 1996; Sölva et al., 2005). Even higher *P-T* conditions are reported for the Texel Nappe with the metamorphic peak of the dominant amphibolite-facies metamorphism at ~90 Ma, ranging between 550 to 650 °C and 8–11 kbar (Hoinkes et al., 1991; Spalla, 1993; Sölva et al., 2001; Tribus, 2008; Zanchetta et al., 2013; Tropper et al., 2023; Lanziner-Oberrauch, 2024). Eclogite relics in metabasites from the Texel Nappe also indicate a pressure-dominated metamorphic stage pre-dating the amphibolite facies stage of Eoalpine metamorphism, with *P-T* conditions of 550–650 °C and 19–22 kbar (Habler et al., 2006; Thöni, 2006; Tribus et al., 2008; Miladinova et al., 2022; Tropper et al., 2023). Zanchetta et al. (2013) even postulated *P-T* conditions of 630–690 °C and 26–29 kbar. In the BM the Eoalpine metamorphic temperatures are ranging from 450 °C in the north to 530 °C in the south (Hoernes and Friedrichsen, 1978; Dietrich, 1983). Similarly, the Eaolpine metamorphic gradient in the Austroalpine units east of the Tauern window shows increasing *P-T* conditions from the north to the south (Faryad and Hoinkes, 2003; Tenczer and Stüwe, 2003; Schorn and Stüwe, 2016; Iglseder et al., 2022; Stumpf et al., 2024).

Tectonically the ÖN is part of the Ötztal-Bundschuh Nappe System following the classification of Schmid et al. (2004). During the Cretaceous in the Eastern Alps a northwest-directed nappe stack evolved, where the Ötztal-Bundschuh Nappe System takes an upper plate position, overriding both the Koralpe-Wölz Nappe System (Schneeberg- and Texel Nappe) and the Silvretta-Seckau Nappe System to which are attributed the Silvretta-, the Sesvenna- and the Campo Nappe. It is assumed that the dipping of the Eoalpine metamorphic gradient towards northwest is attributed to this Cretaceous ramp geometry of the Austroalpine nappe stack and the subsequent Eocene Indentation of the Southalpine Indenter into the Austroalpine nappe stack (Pomella et al., 2016). Therefore, in the northwest shallow crust is exposed, whereas in the southeast at the tip of the Southalpine Indenter structurally deeper crustal levels are exposed.

2. Methods

In total 17 dike samples from the ÖN, one from the TN and one from the SN were analysed with respect to their petrography and mineral chemistry. We used 13 dike samples from the ÖN that Dieter Rammlmair has collected during his dissertation at the University of Innsbruck. In addition, we took four samples from the central and southern ÖN, as well as one sample from the TN (GR13/01) and one sample from the SN (GR144/01). The sample locations and the respective coordinates are given in Figure 2 and Table 1.

The major elements of the metamorphic mineral assemblage were analysed using the JEOL JXA-iSP100 electron probe microanalyzer (EPMA) at the Institute of Mineralogy and Petrography at the University of Innsbruck. For quantitative analysis 5 WDS spectrometers and the following mineral standards containing the elements of interest were used: quartz (Si), corundum (Al), orthoclase (K), diopside (Ca), rutile (Ti), chromite (Cr), rhodonite (Mn), almandine (Fe), jadeite (Na) and periclase (Mg). The measurement conditions were 15 kV and 10 nA. The electron beam was focused down to a spot to prevent mixed analyses. Counting times were 20 s on the peak and 10 s on the background. For each phase of each sample we carried out at least 3 measurements.

Multi-equilibrium geothermobarometry was performed using the programs THERMOCALC v.3.21 (tcds55 data set from 1999), THERMOCALC v.3.33 (tcds55s data set from 2003) and THERMOCALC v.3.45 (tcds62 data set

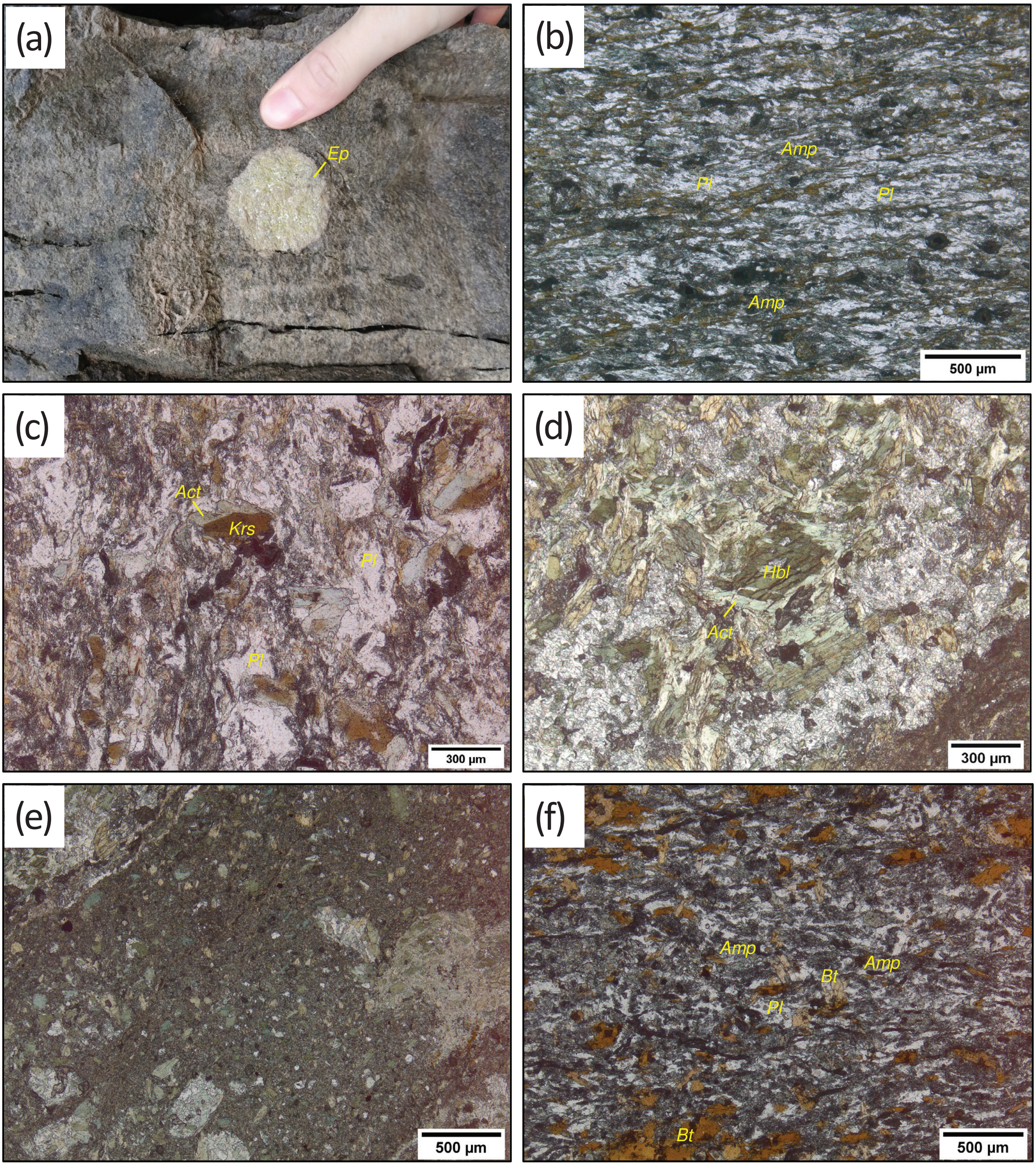

Figure 3: Textures of the investigated dike samples. **(a)** Hand specimen of a dike sample from the SN (GR144/01). This sample is fine grained with a dark grey colour that sometimes contains rounded yellow-green epidote/clinozoisite inclusions. **(b)** Photomicrograph of a dike sample from the northwestern ÖN (RH1). This sample is characterized by a pronounced schistosity formed mostly by amphibole. **(c)** Photomicrograph of a dike sample from the northwestern ÖN (RP4). This sample is characterized by reddish-brown kaersutite crystals surrounded by a rim of pale green actinolite. **(d)** Photomicrograph of a dike sample from the Stubai valley (RE1). This sample is characterized by hornblende crystals surrounded by a rim of actinolite. **(e)** Photomicrograph of a dike sample from the Stubai valley (RE1). This sample contains also fine-grained areas of darker colour with individual larger crystals (up to 200 µm). **(f)** Photomicrograph of a dike sample from the central ÖN (R2S). This sample shows a weak schistosity formed by amphibole and less pronounced by biotite. Sometimes biotite is also developed obliquely to the schistosity and forms clusters of multiple crystals. Mineral abbreviations according to Whitney and Evans (2010): Bt = biotite, Amp = amphibole, Pl = plagioclase, Ep = epidote/clinozoisite, Act = actinolite, Hbl = hornblende, Krs = kaersutite.

from 2012). THERMOCALC is based on an internally consistent thermodynamic database (Holland and Powell, 1998; 2011) coupled with the AX program to calculate the activities of the phase components. The reason of using three different versions of THERMOCALC was to evaluate the influence of amphibole activity models on the calculations. THERMOCALC v.3.21 uses a 2000 version of AX with the amphibole model of Dale et al. (2000), whereas THERMOCALC v.3.33 uses a 2008 version of AX with the amphibole model of Dale et al. (2005) and THERMOCALC v.3.45 uses the 2018 version of AX62 with the amphibole model of Diener et al. (2007). THERMOCALC offers two types of calculations: Mode-2 (average *PT* Mode) calculates an independent set of reactions from the endmembers of the mineral assemblage (Powell and Holland, 2008). Each reaction is assigned a specific *P-T* band, the bands are being correlated to each other via the activities. The results are then combined statistically using the least-squares method to get a best fit of *P-T* estimates. Mode-1 calculations involve only mineral reactions around invariant points in specific chemical systems. For the multi-equilibrium calculations we assumed a H_2O activity of 1.

In addition to multi-equilibrium geothermobarometry we also used classical geothermometers: The hornblende-plagioclase geothermometer by Holland and Blundy (1994) was used on amphibole-plagioclase pairs and the Ti-in-amphibole geothermometers by Colombi (1989), Ernst and Liu (1998) and Liao et al. (2021) were applied on Ca-amphiboles from the metamorphic mineral assemblage. The hornblende-plagioclase geothermometer is calibrated based on the two reactions: (A) edenite + 4 quartz = tremolite + albite and (B) edenite + albite = richterite + anorthite. The Ti-in-amphibole geothermometers were empirically calibrated on the temperature-dependent incorporation of Ti in Ca-amphibole. The advantage of the multi-equilibrium approach over the classical geothermobarometry is that thermodynamic data from all phase components of the equilibrium assemblage are from one internally consistent database and the phase components are considered for the *P-T* calculations within the uncertainty of their activities.

3. Petrography

The northwesternmost dike sample from the SN (GR144/01) is extremely fine grained (~20 µm) and consists of albite + chlorite + quartz + muscovite. This sample sometimes contains rounded yellow-green epidote/clinozoisite inclusions with diameters of 2–3 cm (Fig. 3a). The samples from the northwestern ÖN (RH1, RF5) are fine grained (50–200 µm) and characterized by a pronounced schistosity formed mostly by amphibole (Fig. 3b). The sample RP4 from the northwestern ÖN contains magmatic relics, e.g. reddish-brown kaersutite porphyroclasts surrounded by a rim of pale green actinolite (Fig. 3c). Additionally, it contains the mineral assemblage mentioned above. The sample from the Kauner valley

Sample	Locality	Coordinates Nord	East	Tectonic Unit	Host Rock	Mineral Assemblage	Accessory Minerals	MZ
GR144/01	Landeck	47.138002°N	10.571565°E	SN	quartzphyllite	Ab + Chl + Qz + Ms	Ap + Rt + Zrn + Ilm + Py	1
GR11/40	Langtaufers	46.821395°N	10.590216°E	ÖN	biotite-plagioclase-gneiss	Pl + Ms + Chl + Ep + Ttn + Amp	Ap + Ilm + Py	2
GR11/34	St. Martin, Graun	46.780095°N	10.524618°E	ÖN	orthogneiss	Pl + Kfs + Qz + Ms + Chl + Ep + Ttn	Ap + Stp + Zrn	/
GR12/01	Talatsch, Schlanders	46.642809°N	10.766119°E	ÖN	orthogneiss	Pl + Amp + Bt + Chl + Qz + Ttn + Ep	Ap	5
GR13/01	Tschigot, Partschins	46.720162°N	11.055857°E	TN	orthogneiss of Parcines	Pl + Bt + Amp + Qz + Grt + Chl + Ttn + Ep	Ap	6
RO1	Obergurgl	46.836016°N	11.002215°E	ÖN	biotite-plagioclase-gneiss	Pl + Bt + Amp + Qz + Grt + Ep + Chl	Ap + Rt	6
R2S, GRS/01	Sölden	46.949718°N	11.012802°E	ÖN	gneiss	Pl + Amp + Bt + Chl + Qz + Ms + Ep + Ttn + Kfs	Ap + Zrn	4
R8K, R6K	Kauner valley	46.925310°N	10.744232°E	ÖN	gneiss	Pl + Amp + Bt + Chl + Qz + Ms + Ep + Ttn	Cal	3
R11T	Timmelsjoch	46.900506°N	11.095486°E	ÖN	gneiss, galenite-amphibolite	Pl + Amp + Bt + Qz + Ep + Ttn + Chl + Ms	Ap	5
RE2	Stubai valley	47.066981°N	11.229600°E	ÖN	biotite-plagioclase-gneiss	Pl + Amp + Qz + Bt + Ep + Ttn + Chl		5
RH1	Kühtai	47.229851°N	11.025086°E	ÖN	granite-gneiss, gneiss	Pl + Amp + Qz + Chl + Bt + Ep + Ttn + Ms + Kfs		2
R2D	Pitz valley	47.048304°N	10.873180°E	ÖN	biotite-schist, biotite-gneiss	Pl + Amp + Bt + Chl + Qz + Ep + Ttn + Ms	Ap	3
RE1	Stubai valley	47.121070°N	11.281937°E	ÖN	biotite-plagioclase-gneiss	Pl + Amp + Ms + Chl + Ep + Ttn	Cal + Zrn	4
RF5	Finstertaler Seen	47.185283°N	11.039596°E	ÖN	biotite-plagioclase-gneiss	Pl + Amp + Ms + Chl + Ep + Ttn		3
RP4	Plankogel, Umhausen	47.174472°N	10.953072°E	ÖN	biotite-plagioclase-gneiss	Pl + Amp + Ms + Chl + Ep + Ttn		3
R3W	Bachfallenferner	47.081450°N	11.073197°E	ÖN	migmatite	Pl + Bt + Chl + Qz + Ep + Ttn + Amp		3
RU2	Fotscher valley	47.176661°N	11.190142°E	ÖN	galenite-staurolite-schist	Pl + Amp + Bt + Qz + Chl + Ttn + Ep + Ms		3

Table 1: Mineral assemblage of the dike samples from the ÖN, the Texel Nappe (TN) and the Silvretta Nappe (SN). MZ = metamorphic zones according to Purtscheller and Rammlmair (1982). Mineral abbreviations according to Whitney and Evans (2010): Ab = albite, Pl = plagioclase, Chl = chlorite, Qz = quartz, Ms = muscovite, Ep = epidote/clinozoisite, Ttn = titanite, Amp = amphibole, Kfs = orthoclase, Bt = biotite, Grt = garnet, Ap = apatite, Rt = rutile, Ilm = ilmenite, Py = pyrite, Stp = stilpnomelane, Cal = calcite, Zrn = zircon.

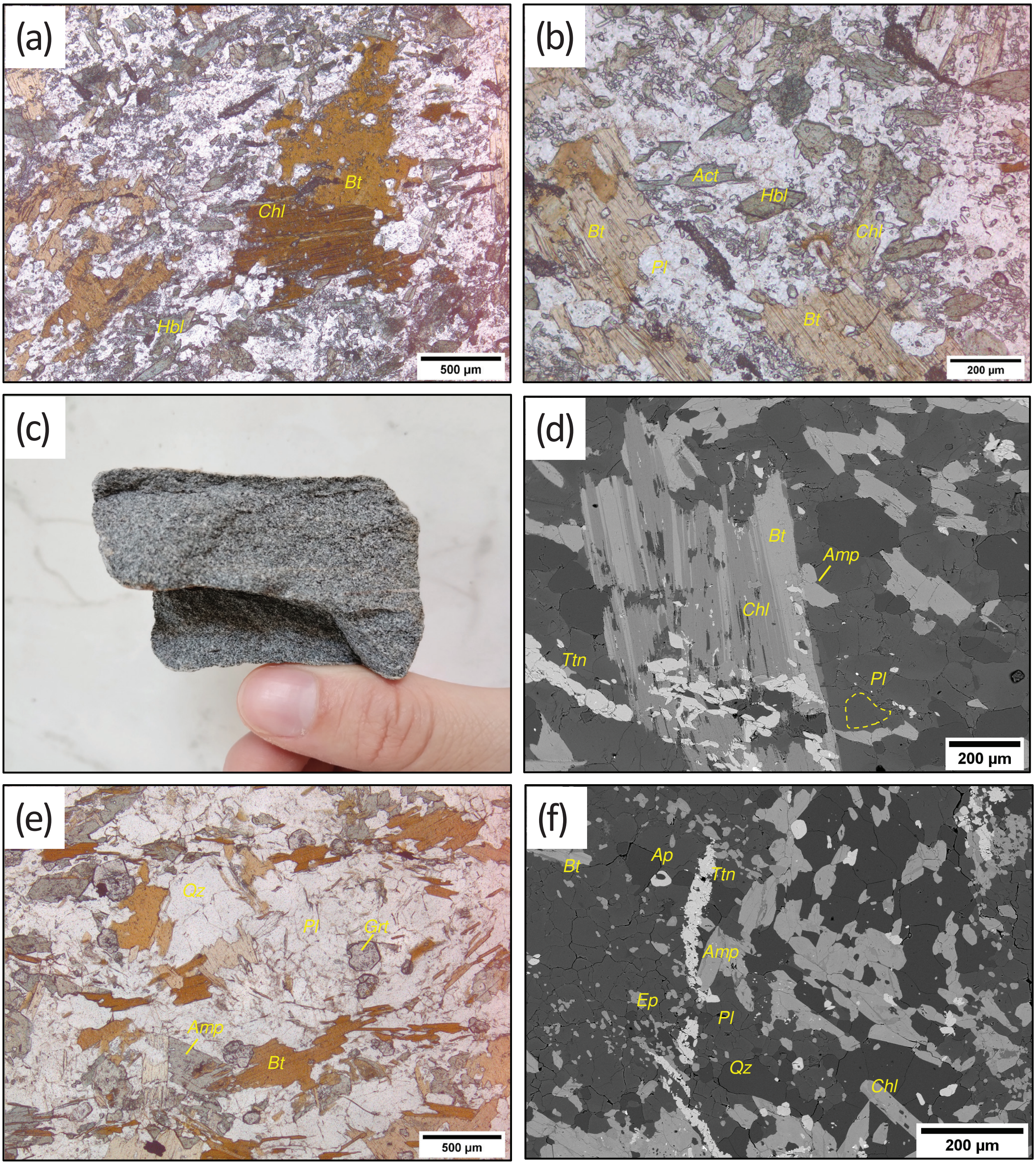

Figure 4: Textures of the investigated dike samples. **(a)** Photomicrograph of a dike sample from the southeastern ÖN (R11T). This sample is coarse grained (up to a few mm) and it only shows a weak schistosity. Biotite has developed large crystals (up to 1 mm) with overgrowths of chlorite. **(b)** Photomicrograph of a dike sample from the southeastern ÖN (R11T). This sample is characterized by the occurrence of two different types of amphiboles: pale green actinolite and grass-green hornblende. **(c)** Hand specimen of a dike sample from the Texel Nappe (GR13/01). This sample is characterized by a pronounced schistosity formed by amphibole and biotite also visible on macroscopic scale. Furthermore, it contains garnet porphyroblasts with grain sizes ranging between 50 and 250 µm. **(d)** Backscattered electron (BSE) image of a dike sample from the TN (GR13/01). Plagioclase at the bottom right of the image shows an internal zonation, titanite forms aggregates of rhomboidal crystals. **(e)** Photomicrograph of a dike sample from the southeastern ÖN (RO1). This sample is characterized by large amphibole and biotite crystals (up to 1 mm) and the occurrence of garnet porphyroblasts. **(f)** Backscattered electron (BSE) image of a dike sample from the southeastern ÖN (R11T). This sample contains the characteristic mineral assemblage. Titanite forms aggregates of rhomboidal crystals, which replace older ilmenite crystals. Mineral abbreviations according to Whitney and Evans (2010): Bt = biotite, Amp = amphibole, Pl = plagioclase, Ep = epidote/clinozoisite, Qz = quartz, Chl = chlorite, Act = actinolite, Hbl = hornblende, Ttn = titanite, Ap = apatite, Grt = garnet.

(R6K), as well as the sample from the Stubai valley (RE1), is characterized by grass-green hornblende crystals surrounded by a rim of actinolite (Fig. 3d). The samples from the Kauner valley (R6K, R8K) and from the Pitz valley (R2D) are characterized by a pronounced schistosity, whereas the sample from the Stubai valley (RE1) has only developed a weak schistosity. This sample also contains fine grained areas of darker colour with individual larger crystals, generally not exceeding 200 µm (Fig. 3e). The sample from the central ÖN (R2S) contains the mineral assemblage plagioclase + amphibole + biotite + chlorite + quartz. It has developed a weak schistosity formed by amphibole and less pronounced by biotite. Sometimes biotite is also developed obliquely to the schistosity and forms clusters of multiple crystals (Fig. 3f). The samples from the southeastern ÖN (RO1, R11T) are coarse grained (up to some mm) and they only show a weak schistosity (Fig. 4a). These samples contain the mineral assemblage plagioclase + amphibole + biotite + quartz. Biotite has developed large crystals (up to 1 mm) with overgrowths of chlorite. In the sample R11T two different types of amphiboles can be observed: pale green actinolite forming typical needles and grass-green hornblende with a well-developed 120° cleavage (Fig. 4b). The sample from the TN (GR13/01) is characterized by a pronounced schistosity formed by amphibole and biotite, visible also on macroscopic scale (Fig. 4c). Plagioclase commonly shows an internal chemical zonation (Fig. 4d). This sample and the sample RO1 from the southeastern ÖN contain garnet porphyroblasts with grain sizes varying between 50 and 250 µm (Fig. 4e). All samples contain as minor component epidote. Epidote has generally an equidimensional shape but develops also prismatic crystals, which sometimes also shows an internal chemical zonation. The main Ti-bearing phase is titanite, which occurs in almost all the samples, with exception of the samples GR144/01 and RO1. Titanite generally forms aggregates of rhomboidal crystals, which sometimes replace older ilmenite crystals (Fig. 4f). Other accessory minerals are rutile, apatite, zircon, pyrite, stilpnomelane and calcite. The most common alteration mineral is chlorite, which forms overgrowths on both amphibole and biotite. Other alteration minerals are sericite and zoisite.

The dike samples are characterized by the occurrence of minerals of their respective metamorphic zone (MZ; Purtscheller and Rammlmair, 1982):

MZ 1: albite + chlorite + stilpnomelane
MZ 2: albite + chlorite + epidote + titanite + actinolite
MZ 3: albite + chlorite + epidote + titanite + actinolite + biotite
MZ 4: albite + chlorite + epidote + titanite + actinolite + biotite + hornblende
MZ 5: oligoclase + biotite + hornblende + chlorite + epidote + titanite
MZ 6: oligoclase + biotite + hornblende + ilmenite + garnet

4. Mineral Chemistry

Plagioclase: The plagioclase composition varies from almost pure albite (X_{An}<0.1) in the northwestern ÖN to plagioclase with an anorthite component X_{An}=0.30-0.35 in the southeastern ÖN (Fig. 5a). Plagioclases from the southeastern ÖN with a compositional zonation show increasing anorthite component from the core to the rim (Tab. 2).

Amphibole: Amphibole shows a compositional variation as a function of metamorphic grade especially in Si, Al and Na. The Si-content varies between 7.50 and 7.88 apfu for the northwestern dike samples and between 6.47 and 6.73 apfu for the southeastern dike samples (Fig. 5b). The Al^{IV}-content varies between 0.12 and 0.50 apfu for the northwestern dike samples and between 1.27 and 1.53 apfu for the southeastern dike samples (Fig. 5c). The Na^{A}-content varies between 0.00 and 0.13 apfu for the northwestern dike samples and between 0.21 to 0.39 apfu for the southeastern dike samples (Fig. 5d). The Al^{VI}-content varies between 0.11 and 0.32 apfu for the northwestern dike samples and between 0.86 and 1.21 apfu for the southeastern dike samples (Fig. 5e). In the ^{A}(Na+K+2Ca) vs. ^{C}(Al+Fe^{3+}+Mn^{3+}+Cr+2Ti) diagram with the stability fields according to Hawthorne et al. (2012) the rim-amphiboles from the northwestern dike samples plot in the actinolite field, whereas the amphiboles from the southeastern dike samples are magnesio-hornblendes (Fig. 5f). This is also shown by the X_{Mg} vs. Si diagram with the stability fields of the amphibole endmembers according to Leake et al. (1997) (Fig. 6a). The glaucophane component according to Schumacher (2007) [GL = Na^{B}] ranges from 0.04 to 0.24 apfu (Fig. 6b). The tschermakite component [TS = Al^{IV}-Na^{A}-K^{A}-2Ca^{A}] ranges from 0.13 to 0.44 for the northwestern dike samples and from 0.99 to 1.32 apfu for the southeastern dike samples (Fig. 6c). The edenite component [ED = Na^{A}+K^{A}+Ca^{A}] varies between 0.00 and 0.12 for the northwestern dike samples and between 0.21 and 0.39 for the southeastern dike samples (Fig. 6d). The glaucophane, the tschermakite and the edenite component in amphibole increase from northwest to southeast within the ÖN. Amphiboles with a compositional zonation show decreasing edenite component from the core to the rim. Also, the Ti-content varies from the core to the rim, ranging between 0.28 apfu in the core and 0.01 apfu in the rim.

Muscovite: The white micas are phengitic with a Si-content ranging between 3.27 and 3.53 apfu. The paragonite component [X_{Pg} = Na/(Na+K)] varies between 0 and 0.32. No systematic chemical variation was found.

Chlorite: The Si-content of chlorite varies between 2.68 and 3.20 apfu (Fig. 6e). The clinochlore component [X_{Clc} = Mg/(Mg+Fe^{2+})] varies between 0.38 and 0.58 for the northwestern dike samples and between 0.52 and 0.64 for the southeastern dike samples (Fig. 6f).

Epidote/Clinozoisite: The epidote component [X_{Ep} = Fe^{3+}/(Fe^{3+}+Al+Cr-2)] varies between 0.02 and 0.86 but no systematic chemical variation was found.

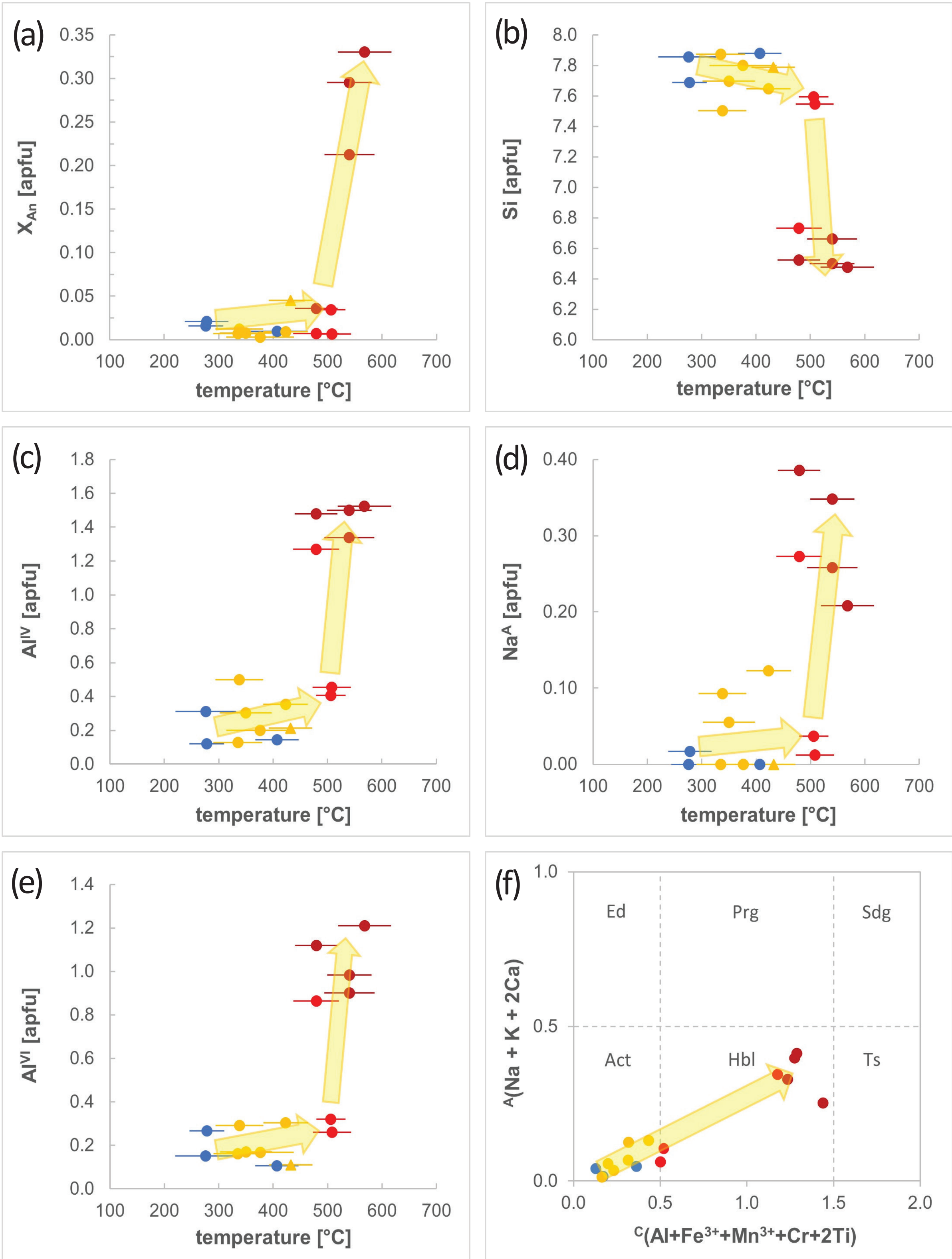

Figure 5: Plagioclase (a) and amphibole (b-f) compositional plots. The data points correspond to a single analysis and the colours represent the spatial distribution of the dike samples as indicated in Figure 2. **(a)** X_{An} in plagioclase vs. temperature [°C]. **(b)** Si in amphibole vs. temperature [°C]. **(c)** Al^{IV} in amphibole vs. temperature [°C]. **(d)** Na^{A} in amphibole vs. temperature [°C]. (e) Al^{VI} in amphibole vs. temperature [°C]. **(f)** $^{A}(Na+K+2Ca)$ vs. $^{C}(Al+Fe^{3+}+Mn^{3+}+Cr+2Ti)$ diagram with the stability fields of the amphibole endmembers according to Hawthorne et al. (2012). The amphiboles from the northwestern dike samples plot in the stability field of actinolite, whereas the amphiboles from the southeastern dike samples are magnesio-hornblendes. The plotted temperatures derive from multi-equilibrium geothermobarometry (circles) and from the hornblende-plagioclase geothermometer (triangle) as discussed in section 5. Mineral abbreviations according to Whitney and Evans (2010): Act = actinolite, Hbl = magnesio-hornblende, Ed = edenite, Ts = tschermakite, Prg = pargasite, Sdg = sadanagaite.

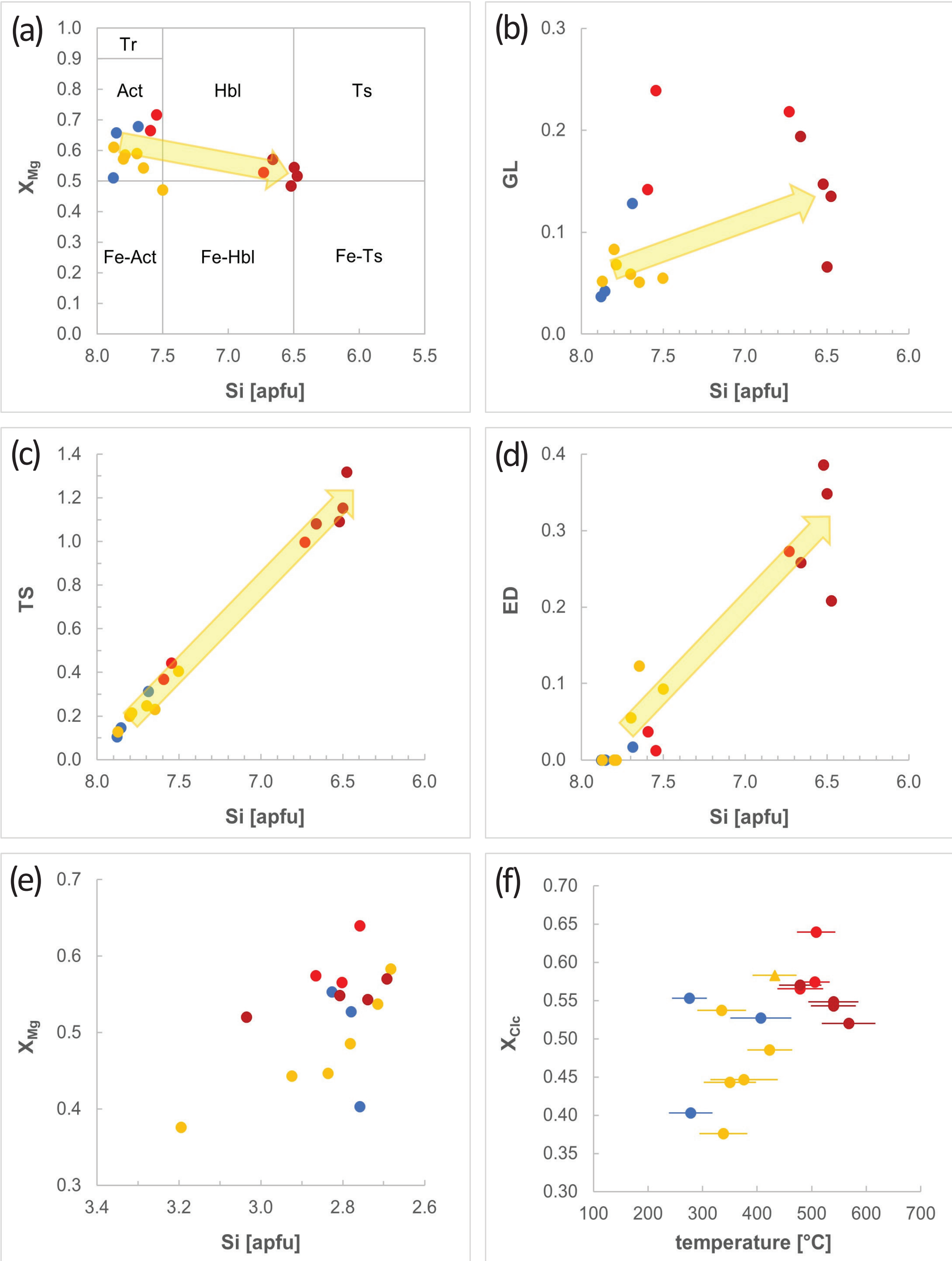

Figure 6: Amphibole (a-d) and chlorite (e-f) compositional plots. The data points correspond to a single analysis and the colours represent the spatial distribution of the dike samples as indicated in Figure 2. **(a)** X_{Mg} vs. Si diagram with the stability fields of the amphibole endmembers according to Leake et al. (1997). The amphiboles from the northwestern dike samples are actinolites, whereas the amphiboles from the southeastern dike samples are magnesio-hornblendes. **(b)** GL vs. Si diagram shows increasing glaucophane component [GL = Na^B] from northwest to southeast of the ÖN. **(c)** TS vs. Si diagram shows increasing tschermakite component [TS = Al^4-Na^A-K^A-$2Ca^A$] from northwest to southeast of the ÖN. **(d)** ED vs. Si diagram shows increasing edenite component [ED = Na^A+K^A+Ca^A] from northwest to southeast of the ÖN. The GL, TS and ED components are according to Schumacher (2007). **(e)** X_{Mg} vs. Si diagram of chlorite. No systematic chemical variation could be found. **(f)** X_{Clc} vs. temperature [°C] shows increasing clinochlore component from northwest to southeast of the ÖN. The plotted temperatures derive from multi-equilibrium geothermobarometry (circles) and from the hornblende-plagioclase geothermometer (triangle) as discussed in section 5. Mineral abbreviations according to Whitney and Evans (2010): Tr = tremolite, Act = actinolite, Hbl = magnesio-hornblende, Ts = tschermakite, Fe-Act = ferro-actinolite, Fe-Hbl = ferro-hornblende, Fe-Ts = ferro-tschermakite, Clc = clinochlore.

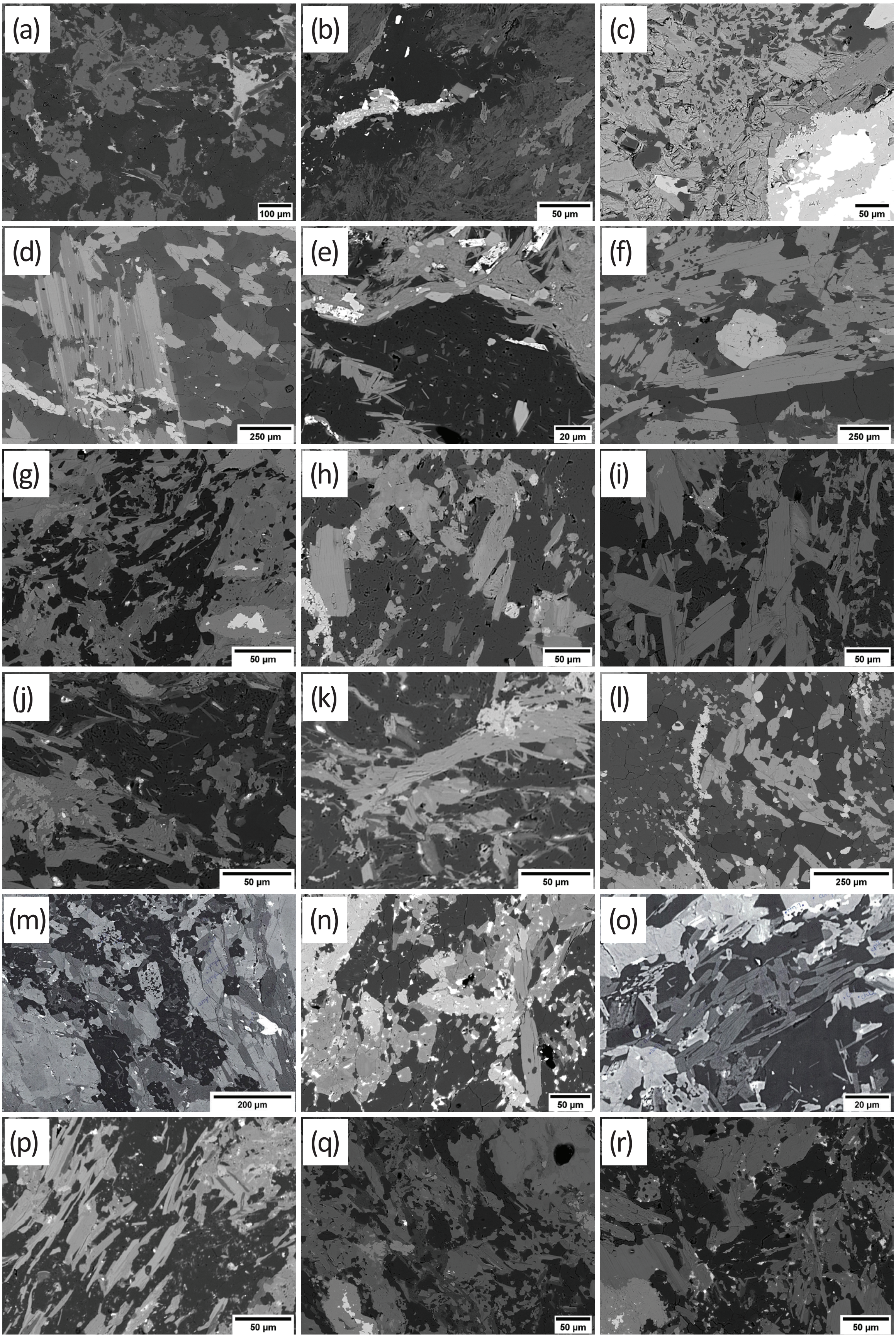

Figure 7: Backscattered electron (BSE) images of the analysed dike samples which indicate the areas used for the geothermobarometric calculations. **(a)** GR11/34, **(b)** GR11/40, **(c)** GR12/01, **(d)** GR13/01, **(e)** GR144/01, **(f)** RO1, **(g)** R2D, **(h)** R2S, **(i)** R3W, **(j)** R6K, **(k)** R8K, **(l)** R11T, **(m)** RE1, **(n)** RE2, **(o)** RF5, **(p)** RH1, **(q)** RP4, **(r)** RU2.

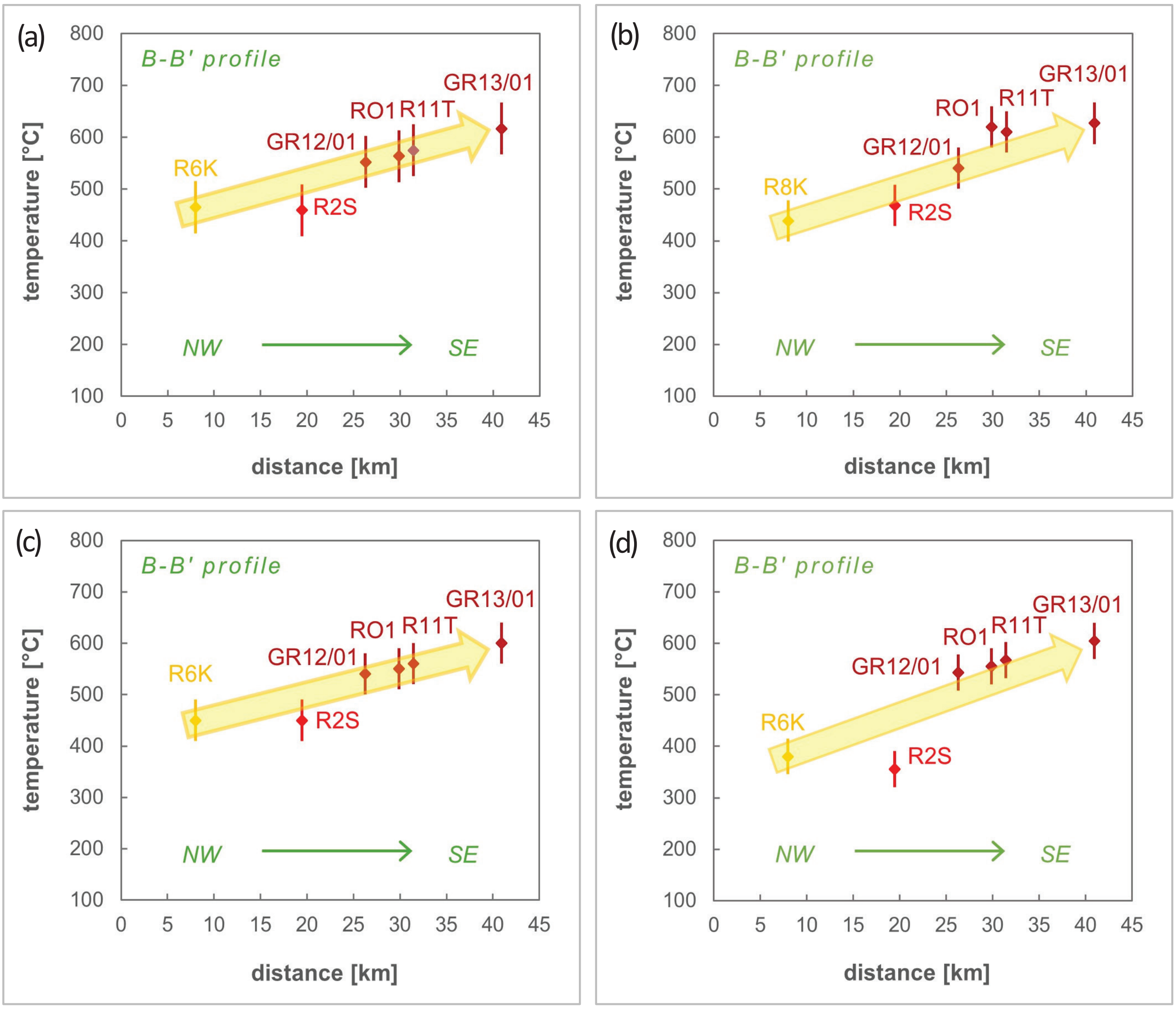

Figure 8: Temperature profiles along a northwest to southeast transect across the Austroalpine units west of the Tauern window (B-B' in Fig. 9a). The colours of the data points represent the spatial distribution of the dike samples as indicated in Figure 2. **(a)** Ti-in-amphibole geothermometer by Colombi (1989). **(b)** Hornblende-plagioclase geothermometer by Holland and Blundy (1994). **(c)** Al_2O_3 vs. TiO_2 geothermobarometer by Ernst and Liu (1998). **(d)** Ti-in-amphibole geothermometer by Liao et al. (2021).

Titanite: The Al-content [X_{Al} = Al/(Al+Ti+Fe^{3+})] ranges from 0.02 to 0.13 for the northwestern dike samples and from 0.04 to 0.07 for the southeastern dike samples. The Fe^{3+}-content [X_{Fe3+} = Fe^{3+}/(Fe^{3+}+Al+Ti)] is low, ranging from 0 to 0.05. Again, no systematic chemical variation was found.

5. Geothermobarometry

5.1. Conventional geothermometry

The geothermobarometric results for the dike samples calculated with the different methods are listed in Table 3. The uncertainties are those given in the respective geothermometer publications. For the calculations, we only considered the rim chemistries of the metamorphic mineral assemblage in textural equilibrium from the same area of the thin section (Fig. 7). The Ti-in-amphibole geothermometer by Colombi (1989) yields metamorphic temperatures of 459–617 ± 50 °C (Fig. 8a) and the hornblende-plagioclase geothermometer by Holland and Blundy (1994) yields metamorphic temperatures of 438–627 ± 40 °C, with increasing temperatures from northwest to southeast (Fig. 8b). These temperatures derive from the edenite-tremolite equilibrium, whereas only a few temperatures could be calculated from the edenite-richterite equilibrium. The calculations with the semiquantitative geothermobarometer by Ernst and Liu (1998) give metamorphic temperatures of 450–600 ± 40 °C (Fig. 8c). The Ti-in-amphibole geothermometer by Liao et al. (2021) results in metamorphic temperatures of 258–605 ± 35 °C (Fig. 8d). By comparing the temperature

	RE1 Amphibole core	rim	Plagioclase	Muscovite	Chlorite	Epidote	Titanite
SiO_2	46.97	52.11	68.57	52.10	26.76	37.91	30.54
TiO_2	0.60	0.07	0.01	0.03	0.01	0.07	36.84
$Al2O_3$	8.98	4.19	19.41	27.33	20.45	24.37	1.77
Cr_2O_3	0.02	0.08	0.01	n.d.	0.14	0.02	0.05
Fe_2O_3	1.99	2.17	0.49	1.96	n.c.	10.65	0.88
FeO	10.19	10.61	n.d.	0.76	19.45	0.40	n.d.
MnO	0.28	0.41	0.03	0.01	0.33	0.16	0.02
MgO	14.02	15.03	0.01	3.95	19.70	n.d.	0.01
CaO	11.70	11.17	0.14	n.d.	0.06	23.03	27.86
Na_2O	1.63	0.89	10.94	0.16	n.d.	0.01	0.03
K_2O	0.41	0.15	0.11	9.95	0.01	0.01	n.d.
Totals	96.79	96.89	99.71	96.25	86.90	96.64	98.00
Si	6.880	7.546	2.999	3.415	2.758	3.033	1.014
Ti	0.066	0.008	n.d.	0.001	0.001	0.004	0.920
Al	1.551	0.715	1.001	2.112	2.485	2.299	0.069
Cr	0.003	0.009	n.d.	n.d.	0.012	0.001	0.001
Fe^{3+}	0.219	0.236	0.016	0.097	n.c.	0.642	0.011
Fe^{2+}	1.249	1.285	n.d.	0.041	1.677	0.027	0.011
Mn	0.035	0.051	0.001	0.001	0.029	0.011	0.001
Mg	3.061	3.244	0.001	0.386	3.026	n.d.	0.000
Ca	1.836	1.733	0.006	n.d.	0.006	1.974	0.991
Na	0.463	0.251	0.928	0.021	n.d.	0.002	0.002
K	0.076	0.028	0.006	0.832	0.001	0.001	n.d.
Sum	15.511	15.183	4.959	6.906	9.993	7.994	3.021
	Mg-Hornblende	Actinolite					
		*X*Ab	0.994				
		*X*An	0.006				
			*X*Pg	0.025			
				*X*Clin	0.639		
				*X*Cham	0.354		
					*X*Ep	0.682	
					*X*Czo/Zo	0.317	
						*X*Al	0.069
						XFe^{3+}	0.011
Oxygens	23	23	8	11	14	13	5

	GR13/01 Amphibole	Plagioclase core	rim	Chlorite	Epidote	Titanite	Biotite
SiO_2	43.85	64.99	61.61	26.08	39.08	30.23	36.97
TiO_2	0.54	0.01	n.d.	0.08	0.04	38.80	2.20
$Al2O_3$	14.22	21.65	24.25	21.20	31.29	1.07	16.52
Cr_2O_3	n.d.	0.01	n.d.	n.d.	0.03	0.01	0.03
Fe_2O_3	1.55	0.05	0.09	n.c.	0.31	n.c.	n.c.
FeO	13.94	n.d.	n.d.	23.41	1.48	0.16	18.23
MnO	0.37	n.d.	0.01	0.34	n.d.	n.d.	0.16
MgO	9.32	n.d.	n.d.	15.84	0.03	n.d.	11.48
CaO	11.19	3.03	6.09	0.02	24.36	28.28	n.d.
Na_2O	1.44	9.86	8.02	0.01	0.02	0.01	0.09
K_2O	0.83	0.10	0.08	0.02	n.d.	0.02	9.44
Totals	97.24	99.70	100.16	86.99	96.63	98.59	95.12
Si	6.499	2.869	2.730	2.739	3.028	1.000	2.803
Ti	0.061	n.d.	n.d.	0.006	0.002	0.965	0.125
Al	2.485	1.127	1.267	2.625	2.858	0.042	1.477
Cr	n.d.	n.d.	n.d.	n.d.	0.002	0.000	0.002
Fe^{3+}	0.173	0.002	0.003	n.c.	0.018	n.c.	n.c.
Fe^{2+}	1.727	n.d.	n.d.	2.057	0.096	0.004	1.156
Mn	0.046	n.d.	n.d.	0.030	n.d.	n.d.	0.011
Mg	2.059	n.d.	n.d.	2.480	0.003	n.d.	1.297
Ca	1.777	0.143	0.289	0.002	2.022	1.002	n.d.
Na	0.414	0.844	0.689	0.002	0.002	0.001	0.013
K	0.157	0.006	0.005	0.002	n.d.	0.001	0.913
Sum	15.455	4.991	4.982	9.944	8.032	3.015	7.796
	Mg-Hornblende						
	*X*Ab	0.855	0.704				
	*X*An	0.145	0.296				
			*X*Clin	0.543			
			*X*Cham	0.450			
				*X*Ep	0.021		
				*X*Czo/Zo	0.977		
					*X*Al	0.041	
					XFe^{3+}	/	
Oxygens	23	8	8	14	13	5	11

	R2S Amphibole rim	Plagioclase	Muscovite	Chlorite	Epidote	Titanite	Biotite
SiO_2	52.03	67.87	48.74	27.33	38.65	30.44	37.19
TiO_2	0.05	n.d.	0.27	0.04	0.08	37.88	1.18
$Al2O_3$	4.21	19.67	29.58	19.28	27.57	1.70	16.57
Cr_2O_3	0.02	n.d.	n.d.	0.01	0.05	0.01	0.02
Fe_2O_3	1.20	0.08	0.40	n.c.	7.15	n.c.	n.c.
FeO	12.42	n.d.	2.32	22.33	0.07	0.39	16.15
MnO	0.37	n.d.	0.03	0.37	0.10	0.04	0.24
MgO	13.87	n.d.	2.70	17.19	0.04	0.01	12.72
CaO	11.67	0.73	n.d.	0.05	23.34	28.46	0.01
Na_2O	0.63	11.18	0.35	0.02	0.02	0.02	0.12
K_2O	0.18	0.07	10.74	0.02	0.01	0.03	9.55
Totals	96.65	99.60	95.14	86.64	97.07	98.97	93.74
Si	7.595	2.979	3.272	2.866	3.028	1.003	2.834
Ti	0.005	n.d.	0.013	0.003	0.005	0.939	0.068
Al	0.725	1.018	2.341	2.383	2.547	0.066	1.489
Cr	0.003	n.d.	n.d.	0.001	0.003	n.d.	0.001
Fe^{3+}	0.131	0.003	0.021	n.c.	0.422	n.c.	n.c.
Fe^{2+}	1.517	n.d.	0.129	1.958	0.004	0.011	1.029
Mn	0.046	n.d.	0.002	0.033	0.007	0.001	0.016
Mg	3.017	n.d.	0.270	2.686	0.005	n.d.	1.444
Ca	1.825	0.034	n.d.	0.006	1.959	1.004	n.d.
Na	0.179	0.951	0.046	0.004	0.002	0.001	0.018
K	0.033	0.004	0.920	0.003	0.001	0.001	0.928
Sum	15.119	4.989	7.017	9.943	7.983	3.027	7.827
	Mg-Hornblende						
	*X*Ab	0.965					
	*X*An	0.035					
		*X*Pg	0.048				
			*X*Clin	0.574			
			*X*Cham	0.419			
				*X*Ep	0.434		
				*X*Czo/Zo	0.563		
					*X*Al	0.066	
					XFe^{3+}	/	
Oxygens	23	8	11	14	13	5	11

	RH1 Amphibole rim	Plagioclase	Muscovite	Chlorite	Epidote	Titanite
SiO_2	52.30	67.93	49.43	25.25	37.83	28.96
TiO_2	0.02	n.d.	0.12	0.03	0.10	35.27
$Al2O_3$	1.28	19.38	26.25	19.92	26.02	1.72
Cr_2O_3	0.02	n.d.	0.02	n.d.	0.01	0.00
Fe_2O_3	0.15	0.26	2.94	n.c.	8.68	0.72
FeO	18.85	n.d.	2.36	29.52	0.38	n.d.
MnO	0.37	n.d.	0.05	0.69	0.17	0.04
MgO	11.02	n.d.	2.98	11.44	0.02	3.80
CaO	11.95	0.44	n.d.	0.03	23.19	26.44
Na_2O	0.18	11.42	0.11	0.01	0.01	0.04
K_2O	0.18	0.09	10.53	0.05	n.d.	0.15
Totals	96.31	99.52	94.79	86.94	96.42	97.14
Si	7.879	2.986	3.354	2.758	3.012	0.972
Ti	0.002	n.d.	0.006	0.003	0.006	0.890
Al	0.227	1.004	2.100	2.565	2.442	0.068
Cr	0.002	n.d.	0.001	n.d.	0.001	0.000
Fe^{3+}	0.017	0.009	0.151	n.c.	0.520	0.018
Fe^{2+}	2.375	n.d.	0.133	2.697	0.025	n.d.
Mn	0.047	n.d.	0.003	0.064	0.012	0.001
Mg	2.474	n.d.	0.301	1.862	0.003	0.190
Ca	1.929	0.021	n.d.	0.003	1.978	0.951
Na	0.054	0.973	0.015	0.001	0.001	0.003
K	0.034	0.005	0.912	0.008	n.d.	0.006
Sum	15.045	4.997	6.978	9.961	8.001	3.099
	Actinolite					
	*X*Ab	0.979				
	*X*An	0.021				
		*X*Pg	0.016			
			*X*Clin	0.403		
			*X*Cham	0.583		
				*X*Ep	0.540	
				*X*Czo/Zo	0.459	
					*X*Al	0.070
					XFe^{3+}	0.019
Oxygens	23	8	11	14	13	5

Table 2: Electron probe microanalyses of four representative dike samples from the ÖN and the Texel Nappe (GR13/01). RE1: Stubai valley, GR13/01: Partschins, R2S: Sölden, RH1: Kühtai. Amphibole: Formula calculation based on 24 anions and 23 oxygens using the excel spreadsheet version 1.9.8 from the amphibole classification of Hawthorne et al. (2012) = IMA 2012. Plagioclase: Formula calculation based on 5 cations and 8 oxygens; Ab = albite, An = anorthite. Muscovite: Formula calculation based on 11 oxygens; Pg = paragonite. Chlorite = Formula calculation based on 10 cations and 14 oxygens; Clc = clinochlore, Chm = chamosite. Epidote = Formula calculation based on 12.5 oxygens; Ep = epidote, Czo/Zo = clinozoisite/zoisite. Titanite: Formula calculation based on 3 cations. Biotite: Formula calculation based on 11 oxygens. Abbreviations: n.d. = not detected, n.c. = not calculated.

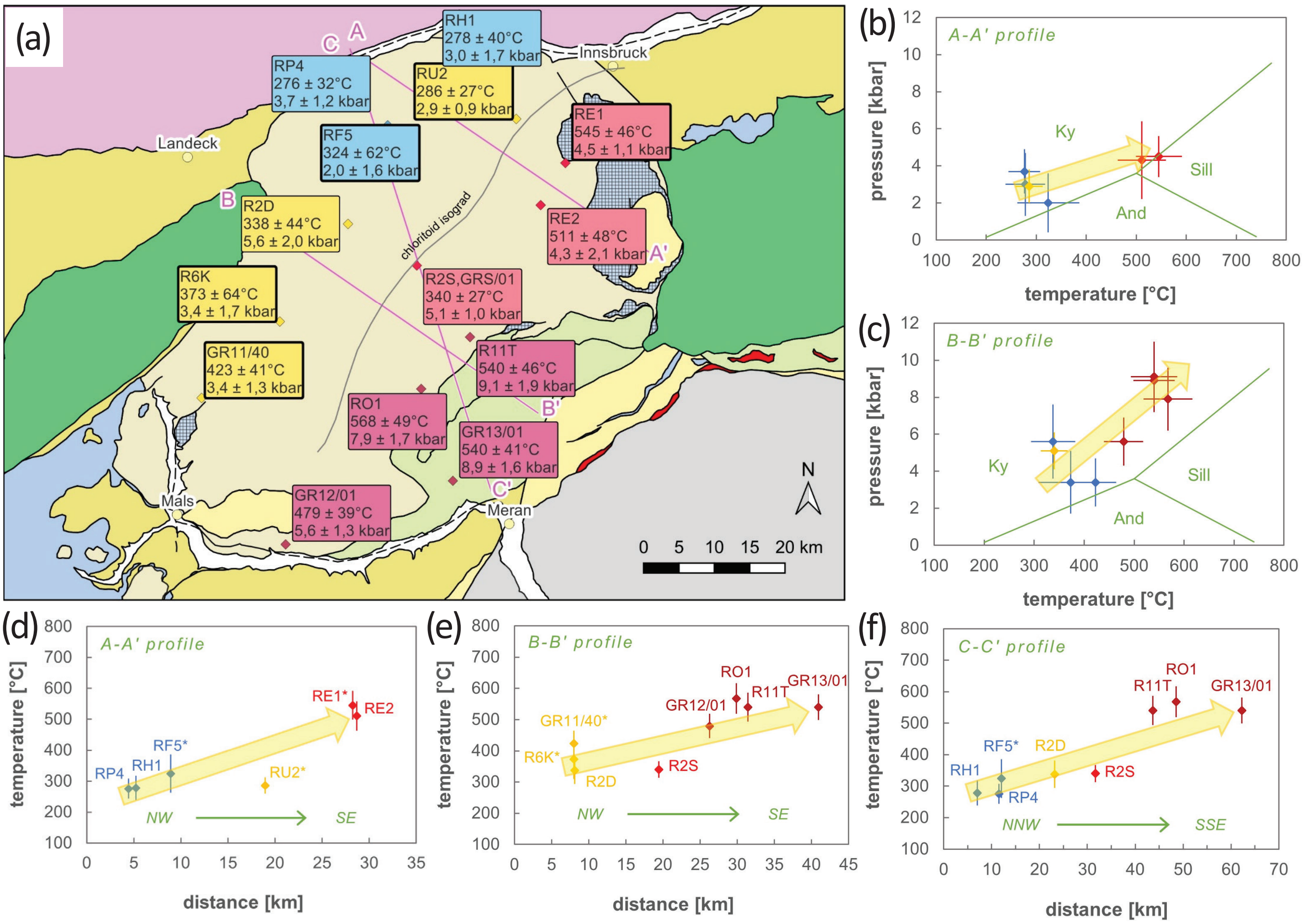

Figure 9: Eoalpine *P-T* conditions in the Austroalpine units west of the Tauern window calculated with THERMOCALC v.3.21. The colours of the data points represent the spatial distribution of the dike samples as indicated in Figure 2. **(a)** Map with Mode-2 (boxes with thin frame) and Mode-1 (boxes with thick frame) calculations. **(b)** *P-T* diagram northern transect A-A'. **(c)** *P-T* diagram central transect B-B'. **(d)** Temperature profile northern transect A-A'. **(e)** Temperature profile central transect B-B'. **(f)** Temperature profile C-C'. The Eoalpine chloritoid isograd after Purtscheller (1967) is given as a grey line.

estimates of individual dike samples, the hornblende-plagioclase geothermometer yields slightly higher temperatures than the Ti-in-amphibole geothermometers.

5.2. Multi-equilibrium geothermobarometry

Multi-equilibrium geothermobarometry was done in the system CaO-FeO-MgO-Na_2O-K_2O-Al_2O_3-SiO_2-H_2O (CFMNKASH) with the mineral assemblage plagioclase + amphibole + chlorite + epidote/clinozoisite + biotite + muscovite + quartz. Due to the rigorous statistical approach and the calculation of linearly independent mineral reactions the focus was on using average *PT* Mode-2 calculations, because they most likely represent robust equilibrium *P-T* conditions. In addition, for some samples it was necessary to use invariant points (Mode-1) instead for the calculations when there were not enough independent mineral equilibria available for the average *PT* Mode.

THERMOCALC v.3.21 yields *P-T* conditions of 276–568 °C and 2.0–9.1 kbar with 1σ-errors of 27–64 °C and 0.9–2.1 kbar (Fig. 9a-c). The *P-T* conditions increase from northwest to southeast of the ÖN. Along the northern transect (A-A') in the ÖN temperatures range from 276 °C in the northwest to 545 °C in the southeast (Fig. 9d). The calculated pressures range from 2.0 kbar in the northwest to 4.5 kbar in the southeast. In the central ÖN (transect B-B') temperatures range from 338 °C in the northwest to 568 °C in the southeast (Fig. 9e). The estimated pressures range from 3.4 kbar in the northwest to 9.1 kbar in the southeast. For 5 out of 14 dike samples invariant point (Mode-1) calculations had to be used (Fig. 10a).

THERMOCALC v.3.33 yields *P-T* conditions of 232–556 °C and 2.4–9.5 kbar with 1σ-errors of 20–89 °C and 0.7–2.9 kbar (Fig. 10b). In the northern ÖN (transect A-A') temperatures range from 254 °C in the northwest to 479 °C in the southeast. The estimated pressures range from 2.5 kbar in the northwest to 4.2 kbar in the southeast. In the central ÖN (transect B-B') temperatures range from 286 °C in the northwest to 556 °C in the southeast. The calculated pressures vary between 2.4 kbar in the northwest and 9.5 kbar in the southeast. For 6 out of 15 dike samples calculations using invariant points (Mode-1) had to be done.

THERMOCALC 3.45 yields *P-T* conditions of 335–636 °C and 2.2–9.3 kbar with 1σ-errors of 32–63 °C and 0.9–2.2 kbar (Fig. 10c). In the northern ÖN (transect A-A') temperatures range from 357 °C in the northwest to 508 °C in the southeast. The estimated pressures vary between 3.1 kbar in the northwest and 8.7 kbar in the southeast. In the central ÖN (transect B-B') temperatures range from 376 °C in the northwest to 636 °C in the southeast. The estimated pressures vary between 2.2 kbar in the northwest to 9.3 kbar in the southeast. For 3 out of 13 dike samples invariant point (Mode-3) calculations were performed.

6. Discussion

Purtscheller and Rammlmair (1982) constrained the increasing grade of Eoalpine metamorphism from northwest to southeast based on the mineralogy as well as the mineral chemistry of plagioclase and amphibole from metamorphosed mafic dikes. In this study we can confirm that the anorthite content (X_{An}) in plagioclase and the tschermakite and edenite component in Ca-amphibole is concordant with increasing *P-T* conditions from northwest to southeast. This can be achieved through the following mineral reaction:

albite + chlorite + epidote + actinolite = hornblende + plagioclase.

We attribute the occurrence of magnesio-hornblende in the core of actinolite to an advanced stage of the magmatic crystallisation, where Ti-rich hornblende (i.e. kaersutite) is formed from Ti-augite. On the other site, magnesio-hornblende without any chemical zonation has only been observed in the dikes from the southeastern ÖN and the TN. Together with the occurrence of garnet porphyroblasts this points to a predominant amphibolite-facies metamorphism in the southeastern ÖN and in the Texel Nappe.

We noticed that the hornblende-plagioclase geothermometer by Holland and Blundy (1994), the Ti-in-amphibole geothermometer by Colombi (1989) and the Al_2O_3 vs. TiO_2 geothermobarometer by Ernst and Liu (1998) are limited by a lower temperature limit of ca. 450 °C, because the required element contents are too low. However, these geothermometers yield reasonable temperature estimates for the dike samples with comprising assemblages of upper greenschist to epidote-amphibolite facies. The Ti-in-amphibole geothermometer by Liao et al. (2021) is applicable on a wider temperature range, including also the lower greenschist facies in the northwest. In comparison, the hornblende-plagioclase geothermometer yields slightly higher temperatures than the Ti-in-amphibole geothermometers.

By using multi-equilibrium geothermobarometry with THERMOCALC we were able to obtain robust *P-T* results, except for three dike samples due to the lack of sufficient mineral phases (e.g. amphiboles) for the calculations.

Sample	Locality	Tectonic Unit	TC 3.21						TC 3.33						TC 3.45						Hb-Pl	Colombi 1989	Ernst & Liu 1998	Liao et al. 2021
			T [°C]	P [kbar]	Mode	Nr.	cor	sigfit	T [°C]	P [kbar]	Mode	Nr.	cor	sigfit	T [°C]	P [kbar]	Mode	Nr.	cor	sigfit	T [°C]	T [°C]	T [°C]	T [°C]
GR144/01	Landeck	SN							374 ± 112	4.3 ± 1.5	M1	3	0.941											
GR11/40	Langtaufers	ÖN	423 ± 41	3.4 ± 1.3	M1	5	0.785		460 ± 39	2.4 ± 1.7	M1	4	0.833		399 ± 33	2.2 ± 1.2	M3	6	0.462					
GR11/34	St. Martin, Graun	ÖN																						
GR12/01	Talatsch, Schlanders	ÖN	479 ± 39	5.6 ± 1.3	M2	3	0.608	0.33							502 ± 44	9.3 ± 1.6	M2	5	0.806	1.58	540 ± 40	552 ± 50	540 ± 50	543 ± 35
GR13/01	Tschigot, Partschins	TN	540 ± 41	8.9 ± 1.6	M2	7	0.960	1.28	545 ± 52	8.7 ± 2.0	M2	4	0.979	0.51	572 ± 35	8.4 ± 1.1	M2	5	0.970	0.97	627 ± 40	617 ± 50	600 ± 50	605 ± 35
RO1	Obergurgl	ÖN	568 ± 49	7.9 ± 1.7	M2	8	0.969	1.46	549 ± 89	6.7 ± 2.9	M2	6	0.982	2.02	636 ± 53	9.0 ± 1.6	M2	6	0.983	0.91	620 ± 40	563 ± 50	550 ± 50	556 ± 35
R2S, GRS/01	Sölden	ÖN	340 ± 27	5.1 ± 1.0	M2	6	0.851	0.62	506 ± 27	5.5 ± 0.9	M2	6	0.742	0.68	518 ± 38	7.5 ± 0.9	M2	5	0.741	0.68	468 ± 40	459 ± 50	450 ± 50	355 ± 35
R8K	Kauner valley	ÖN	350 ± 48	6.8 ± 1.9	M2	5	0.624	1.54	433 ± 64	7.6 ± 1.6	M2	3	0.849	0.97	400 ± 48	4.5 ± 1.9	M3	2	0.818		438 ± 40			425 ± 35
R6K	Kauner valley	ÖN	373 ± 64	3.4 ± 1.7	M1	3	0.896		498 ± 42	4.9 ± 2.0	M1	4	0.819		376 ± 62	4.1 ± 1.4	M3	4	0.677			465 ± 50	450 ± 50	380 ± 35
R11T	Timmelsjoch	ÖN	540 ± 46	9.1 ± 1.9	M2	7	0.930	1.51	556 ± 54	9.5 ± 2.2	M2	4	0.961	0.67	550 ± 32	7.8 ± 1.0	M2	6	0.938	0.95	610 ± 40	575 ± 50	560 ± 50	567 ± 35
RE2	Stubai valley	ÖN	511 ± 48	4.3 ± 2.1	M2	7	0.732	1.59	479 ± 42	3.8 ± 1.8	M2	4	0.722	1.10	447 ± 63	8.7 ± 1.1	M2	4	-0.067	0.92		535 ± 50	520 ± 50	523 ± 35
RH1	Kühtai	ÖN	278 ± 40	3.0 ± 1.7	M2	7	0.901	1.42	254 ± 31	2.5 ± 1.1	M1	5	0.948		357 ± 42	5.4 ± 1.4	M2	4	0.907	1.02				
R2D	Pitz valley	ÖN	338 ± 44	5.6 ± 2.0	M2	4	0.935	0.28	286 ± 41	3.5 ± 1.6	M1	5	0.961											391 ± 35
RE1	Stubai valley	ÖN	545 ± 46	4.5 ± 1.1	M1	6	0.770		443 ± 75	4.2 ± 2.7	M2	3	0.731	1.96	508 ± 35	5.3 ± 1.9	M2	5	0.495	1.34		468 ± 50	460 ± 50	391 ± 35
RF5	Finstertaler Seen	ÖN	324 ± 62	2.0 ± 1.6	M1	3	0.912		439 ± 34	4.3 ± 1.9	M1	2	0.689		407 ± 56	3.1 ± 1.3	M2	3	0.629	0.73				
RP4	Plankogel, Umhausen	ÖN	276 ± 32	3.7 ± 1.2	M2	4	0.876	1.00	312 ± 34	5.4 ± 1.1	M2	5	0.872	0.83							438 ± 40			321 ± 35
R3W	Bachfallenferner	ÖN																			432 ± 40			296 ± 35
RU2	Fotscher valley	ÖN	286 ± 27	2.9 ± 0.9	M1	4	0.731		232 ± 40	2.4 ± 1.1	M2	4	0.750	1.08	335 ± 45	5.1 ± 1.1	M2	4	0.700	0.69				258 ± 35

Table 3: Summary of the calculated *P-T* conditions obtained with the different methods. Abbreviations: TC = THERMOCALC, Hb-Pl = hornblende-plagioclase geothermometer by Holland and Blundy (1994), Nr. = number of independent reactions.

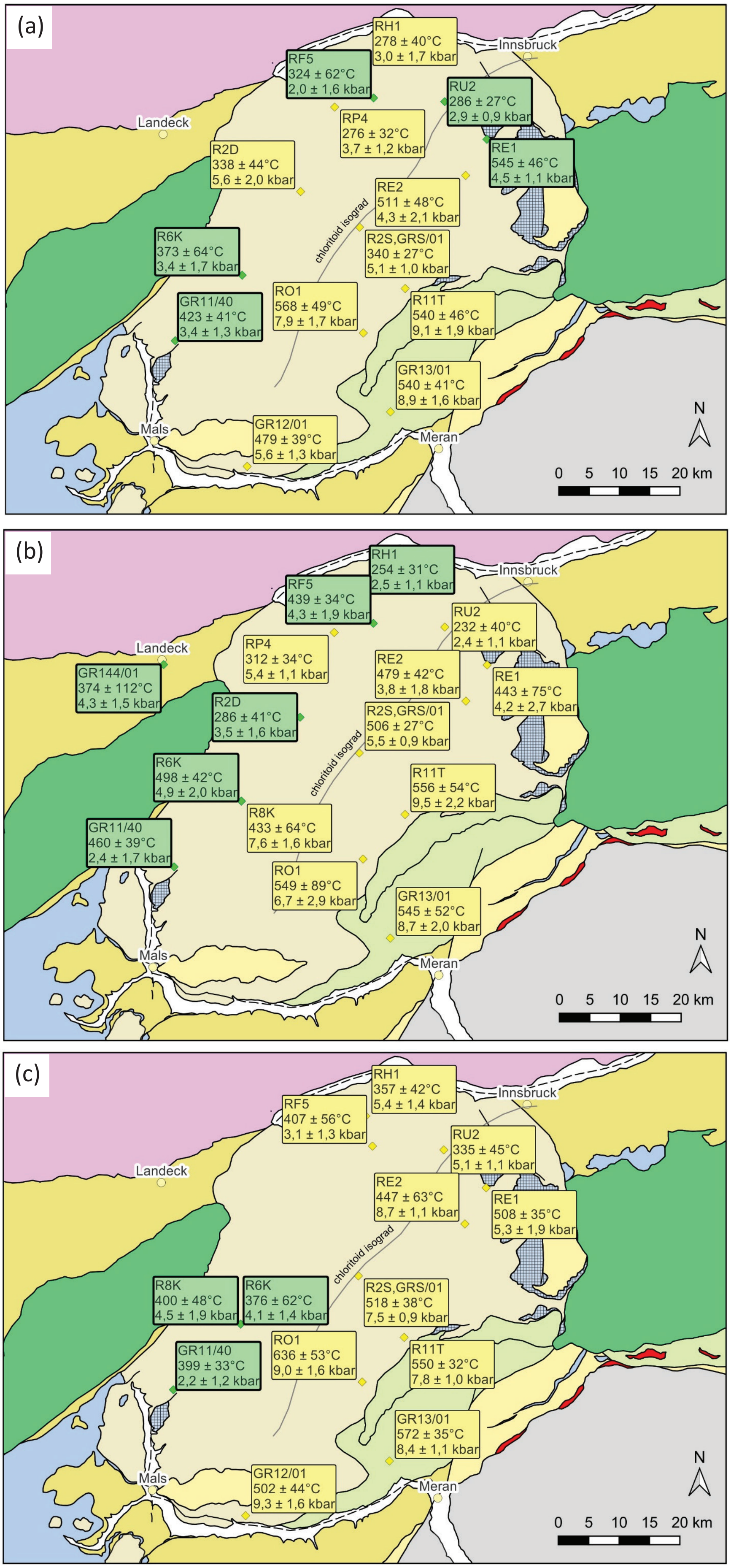

Figure 10: Eoalpine *P-T* conditions in the Austroalpine units west of the Tauern window. **(a)** Map with Mode-2 (yellow boxes) and Mode-1 (green boxes) THERMOCALC v.3.21 calculations. **(b)** Map with Mode-2 (yellow boxes) and Mode-1 (green boxes) THERMOCALC v.3.33 calculations. **(c)** Map with Mode-2 (yellow boxes) and Mode-3 (green boxes) THERMOCALC v.3.45 calculations. The Eoalpine chloritoid isograd after Purtscheller (1967) is given as a grey line.

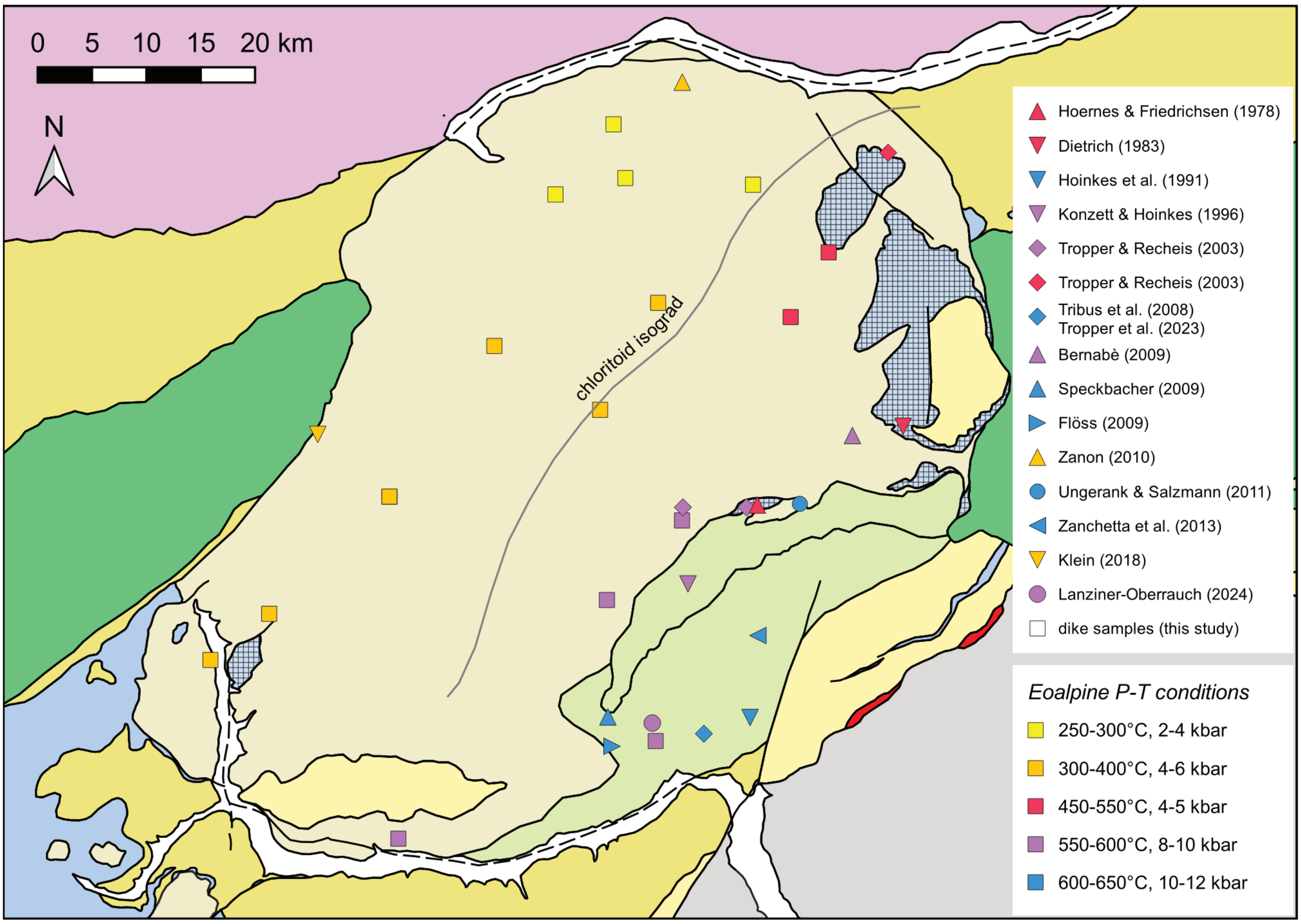

Figure 11: *P-T* constraints for the northwest to southeast trending Eoalpine metamorphic field gradient in the Austroalpine units west of the Tauern window. The *P-T* conditions in the Texel Nappe are of the dominant amphibolite facies metamorphism of the post-eclogitic stage. The Eoalpine chloritoid isograd after Purtscheller (1967) is given as a grey line.

Between the three THERMOCALC versions the following differences could be observed: THERMOCALC v.3.45 calculates slightly higher *P-T* conditions than THERMOCALC v.3.21 and THERMOCALC v.3.33 but corresponds to the calculations with the hornblende-plagioclase and the Ti-in-amphibole geothermometers. This is probably due to the higher glaucophane and the lower tremolite activity calculated with the amphibole model of Diener et al. (2007) used in the AX62 program of THERMOCALC v.3.45. The calculations with THERMOCALC v.3.33 yield the largest 1σ uncertainties of 20–89 °C and 0.7–2.9 kbar, followed by the other two THERMOCALC versions with 1σ uncertainties of ca. 30–60 °C and 1–2 kbar. Tropper et al. (2023) attributes the high standard deviations of the THERMOCALC v.3.33 calculations to slight modifications in the continuously refined thermodynamic data of the internally consistent databases. Since the geothermobarometric calculations with THERMOCALC v.3.33 yield high 1σ uncertainties, we consider that THERMOCALC v.3.21 with the amphibole activity model of Dale et al. (2000) and THERMOCALC v.3.45 with the amphibole activity model of Diener et al. (2007) provide the most robust results.

Our geothermobarometric calculations represent the first quantitative *P-T* constraints for the complete northwest to southeast trending Eoalpine metamorphic gradient in the Austroalpine units west of the Tauern window above and below the chloritoid isograd after Purtscheller (1967). We obtain *P-T* conditions of 250–300 °C and 2–4 kbar for the northern ÖN and 300–400 °C and 4–6 kbar for the western ÖN in Kauner valley, Pitz valley and Langtaufers (Fig. 13). Zanon (2010) calculated similar pressures of 3–4 kbar and slightly higher temperatures of 300–350 °C for phyllites from the northern ÖN using the muscovite-chlorite-plagioclase-quartz geothermobarometer by Vidal and Parra (2000). Since we could not calculate any reliable *P-T* data for the dike sample from the SN (GR144/01), it was not possible to correlate the two adjacent tectonic units with each other. The geothermobarometric results from the southeastern ÖN and from the Stubai valley, below the Mesozoic succession of the "Kalkkögel", agree with previous *P-T* estimates by Tropper and Recheis (2003). They have performed multi-equilibrium geothermobarometry with THERMOCALC v.2.7 (Holland, 1999; written comm.) on metapelites with the mineral assemblage garnet + biotite + plagioclase + muscovite +

quartz. Compared to our approach of using Mode-1 and Mode-2 calculations, they only used Mode-1 calculations. For the southeastern ÖN they have obtained 550–600 °C and 7.2–8.8 kbar, for the northeastern ÖN, underneath the "Kalkkögel" succession, they have obtained 469 ± 56 °C and 4.2 ± 0.9 kbar. Together with the temperature estimates by Hoernes and Friedrichsen (1978) and Dietrich (1983) for the BM *P-T* conditions of 450–550 °C and 4–5 kbar can be attributed to the northeastern ÖN. The *P-T* estimates for the dike sample from the TN (GR13/01: 540 ±4 1 °C, 8.9 ± 1.6 kbar) corresponds to the *P-T* estimates of 550–600 °C and 8–10 kbar obtained by Lanziner-Oberrauch (2024, unpublished M.Sc. thesis) for a metapelitic sample approximately 1.5 km north of the dike location. Further to the east Hoinkes et al. (1991), Tribus et al. (2008) and Tropper et al. (2023) obtained *P-T* conditions of 600–650 °C and 10–11 kbar for amphibolite samples from the Saltaus and the Spronser valley near to the southeastern border of the Texel Nappe. The same *P-T* conditions have also been obtained by several authors from other locations within the TN (Spalla, 1993; Sölva et al., 2001; Zanchetta et al., 2013; Lanziner-Oberrauch, 2024). Our geothermobarometric results point to a predominant Eoalpine amphibolite facies metamorphism in the southeastern ÖN and in the TN and they agree with the already published *P-T* data from this area. Also, we could not find any evidence of the pressure-accentuated eclogite facies stage of metamorphism in the dike from the TN. This demonstrates once more the increase of the Eoalpine metamorphic gradient from the lower greenschist facies in the northwest to the amphibolite facies in the southeast in the Austroalpine units west of the Tauern window.

7. Conclusions

Our geothermobarometric results provide for the first time a continuous profile for the northwest to southeast trending Eoalpine metamorphic gradient in the Austroalpine units west of the Tauern window. In the northwestern ÖN we obtained *P-T* conditions of 250–300 °C and 2–4 kbar, reaching 550–600 °C and 8–10 kbar in the southeastern ÖN, near to the Schneeberg Nappe. In the southerly adjacent TN we obtained 540±41 °C and 8.9 ± 1.6 kbar. The observed Eoalpine metamorphic gradient is consistent with this Cretaceous ramp geometry of the Austroalpine nappe stack and the subsequent Eocene Indentation of the Southalpine Indenter into the Austroalpine nappe stack (Pomella et al., 2016).

Acknowledgements

This research has been supported by the Autonomous Province of Bolzano/Bozen – South Tyrol (Amt für Geologie und Baustoffprüfung) and benefited from financial support from the federal state of Tyrol (research grant Hannah Pomella). The authors wish to thank Volkmar Mair, Corrado Morelli and Daniel Costantini for their support in the field. Silvia Favaro and Luca Toffolo are thanked for providing us one of their samples. Julia Wallraf is thanked for the preparation of the thin sections and Martina Tribus for her help with the electron microprobe. We thank Benjamin Huet and an unknown reviewer for their useful comments, as well as Kurt Stüwe for his throughout editorial handling and his careful suggestions.

References

Ampferer O., Hammer W., 1924. Erläuterungen zur Geologischen Spezialkarte der Republik Osterreich, Blatt Landeck (5145). Geologische Bundesanstalt Wien.

Behrmann J.H., 1988. Crustal-scale extension in a convergent orogen: the Sterzing-Steinach mylonite zone in the Eastern Alps. Geodinamica Acta (Paris) 2, 63–73. https://doi.org/10.1080/09853111.1988.11105157

Bernabè E., 2009. Petrologische und thermobarometrische Untersuchungen am Pflerscher Metabasit-Komplex (Pflerschtal, Südtirol, Italien). Diploma thesis, Univ. Innsbruck.

Colombi R., 1989. Metamorphisme et Geochemie des Roches Mafiques des Alpes Ouest-Centrales (Geoprofil Viege-Domodossola-Locarno). Ph.D. Thesis, Univ. Lausanne.

Dale J., Holland T.J.B., Powell R., 2000. Hornblende-garnet-plagioclase thermobarometry: a natural assemblage calibration of the thermodynamics of hornblende. Contributions to Mineralogy and Petrology 140, 353–362. https://doi.org/10.1007/s004100000187

Dale J., Powell R., White R.W., Elmer F.L., Holland T.J.B., 2005. A thermodynamic model for Ca-Na clinoamphiboles in Na_2O-CaO-FeO--MgO-Al_2O_3-SiO_2-H_2O-O for petrological calculations. Journal of Metamorphic Geology 238, 771–791. https://doi.org/10.1111/j.1525-1314.2005.00609.x

Diener J.F.A., Powell R., White R.W., Holland T.J.B., 2007. A new thermodynamic model for clino- and orthoamphiboles in the system Na_2O-CaO-FeO-MgO-Al_2O_3-SiO_2-H_2O-O. Journal of Metamorphic Geology 25, 631–656. https://doi.org/10.1111/j.1525-1314.2007.00720.x

Dietrich H., 1983. Zur Petrologie und Metamorphose des Brennermesozoikums (Stubaier Alpen, Tirol). Tschermaks mineralogische und petrographische Mitteilungen 31, 235–257. https://doi.org/10.1007/BF01081371

Ernst W.G., Liu J., 1998. Experimental phase-equilibrium study of Al- and Ti-contents of calcic amphibole in MORB - A semiquantitative thermobarometer. American Mineralogist 83, 952–969. https://doi.org/10.2138/am-1998-9-1004

Faryad S.W., Hoinkes G., 2003. P-T gradient of Eo-Alpine metamorphism within the Austroalpine basement units east of the Tauern Window (Austria). Mineralogy and Petrology 77, 129–159. https://doi.org/10.1 007/s00710-002-0196-1

Flöss D., 2009. Tektonometamorphe Entwicklung der westlichen austroalpinen Einheiten: Geometrie und Kinematik der eoalpinen Kollision (Texel Komplex, Südtirol). Diploma thesis, Univ. Innsbruck.

Habler G., Thöni M., Sölva H., 2006. Tracing the high pressure stage in the polymetamorphic Texel Complex (Austroalpine basement Unit, Eastern Alps): P-T-t-d constraints. Mineralogy and Petrology 88, 269–296. https://doi.org/10.1007/s00710-006-0143-7

Habler G., Thöni M., Grasemann, B., 2009. Cretaceous metamorphism in the Austroalpine Matsch Unit (Eastern Alps): the interrelation between deformation and chemical equilibration processes. Mineralogy and Petrology 97, 149–171. https://doi.org/10.1007/s00710-009-0094-x

Hammer W. 1929. Erläuterungen zur Geologischen Spezialkarte der Republik Österreich, Blatt Ötztal (5146). Geologische Bundesanstalt Wien.

Harre W., Kreuzer H., Lenz H., Müller P., Wendt I., Schmidt K., 1968. Rb/Sr- und K/Ar-Altersbestimmungen an Gesteinen des Ötztalkristallins (Ostalpen). Geol. Jb. 86, 797–826.

Hawthorne F.C., Oberti R., Harlow G.E., Maresch W.V., Martin R.F., Schumacher J.C., Welch M.D., 2012. Nomenclature of the amphibole supergroup. American Mineralogist 97, 2031–2048. https://doi.org/10.2138/am.2012.4276

Hoernes S., Friedrichsen H., 1978. Oxygen and hydrogen isotope study of the polymetamorphic area of the northern Ötztal-Stubai Alps (Tyrol). Contributions to Mineralogy and Petrology 67, 305–315. https://doi.org/10.1007/BF00381458

Hoinkes G., 1981. Mineralreaktionen und Metamorphosebedingungen in Metapeliten des westlichen Schneebergerzuges und des angrenzenden Altkristallins (Ötztaler Alpen). Tschermaks mineralogische und petrographische Mitteilungen 28, 31–54. https://doi.org/10.1007/BF01081849

Hoinkes G., Kostner A., Thöni M., 1991. Petrologic constraints for Eoalpine eclogite facies metamorphism in the Austroalpine Ötztal basement. Mineralogy and Petrology 43, 237–254. https://doi.org/10.1007/BF01164529

Holland T.J.B., Blundy J., 1994. Non-ideal interactions in calcic amphiboles and their bearing on amphibole-plagioclase thermometry. Contributions to mineralogy and petrology 116, 433–447. https://doi.org/10.1007/BF00310910

Holland T.J.B., Powell R., 1998. An internally consistent thermodynamic data set for phases of petrological interest. Journal of Metamorphic Geology 16, 309–343. https://doi.org/10.1111/j.1525-1314.1998.00140.x

Holland T.J.B., Powell R., 2011. An improved and extended internally consistent thermodynamic dataset for phases of petrological interest, involving a new equation of state for solids. Journal of metamorphic Geology 29, 333–383. https://doi.org/10.1111/j.1525-1314.2010.00923.x

Konzett J., Hoinkes G., 1996. Paragonite–hornblende assemblages and their petrological significance: an example from the Austroalpine Schneeberg Complex, Southern Tyrol, Italy. Journal of Metamorphic Geology 14, 85–101. https://doi.org/10.1111/j.1525-1314.1996.00085.x

Iglseder C., Rantitsch G., Stumpf S., Skrzypek E., Schuster R., Huet B., 2022. An adapted tectonic model for the "Central and Eastern Greywacke Zone" - new geochronological and RSCM-data (Styria/Austria). Berichte der Geologischen Bundesanstalt 143, 83.

Kübler H., Müller W.E., 1962. Die Geologie des Brenner-Mesozoikums zwischen Stubai-und Pflerschtal (Tirol). Jahrbuch Geologische Bundesanstalt 105, 173–242.

Lanziner-Oberrauch J., 2024. Tektono-metamorphe Charakterisierung des südöstlichen Ostalpins (Ötztal Komplex, Schneeberger Zug, Texel Komplex) in Südtirol, Norditalien. Unpublished M. Sc. thesis, University of Innsbruck.

Leake B.E., Woolley A.R., Arps C.E., Birch W.D., Gilbert M.C., Grice J.D., Hawthorne F.C., Kato A., Kisch H.J., Krivovichev V.G., Linthout K., Laird J., Mandarino J., Maresch W.V., Nickel E.H., Schumacher J.C., Smith D.C., Stephenson N.C.N., Ungaretti L., Whittaker E.J.W., Youzhi G., 1997. Nomenclature of amphiboles; report of the Subcommittee on Amphiboles of the International Mineralogical Association Commission on new minerals and mineral names. Mineralogical magazine 61, 295–310. https://doi.org/10.1127/ejm/9/3/0623

Liao Y., Wei C., Rehman H.U., 2021. Titanium in calcium amphibole: Behavior and thermometry. American Mineralogist 106, 180–191. https://doi.org/10.2138/am-2020-7409

Maggetti M., Flisch M., 1993. Evolution of the Silvretta nappe. In: Pre-Mesozoic geology in the Alps. Springer Berlin Heidelberg, Berlin, 469–484. https://doi.org/10.1007/978-3-642-84640-3_28

Miladinova I., Froitzheim N., Nagel T.J., Janák M., Fonseca R.O., Sprung P., Münker C., 2022. Constraining the process of intracontinental subduction in the Austroalpine Units: Implications from petrology and Lu-Hf geochronology of eclogites. Journal of Metamorphic Geology 40, 423–456. https://doi.org/10.1111/jmg.12634

Miller C., Thöni M., 1995. Origin of eclogites from the Austroalpine Ötztal basement (Tirol, Austria): geochemistry and Sm-Nd vs. Rb-Sr isotope systematics. Chemical Geology 122, 199–225. https://doi.org/10.1016/0009-2541(95)00033-I

Montemagni C., Zanchetta S., Rocca M., Villa I.M., Morelli C., Mair V., Zanchi A., 2023. Kinematics and time-resolved evolution of the main thrust-sense shear zone in the Eo-Alpine orogenic wedge (the Vinschgau Shear Zone, eastern Alps). Solid Earth 14, 551–570. https://doi.org/10.5194/se-14-551-2023

Ortner H., Reiter F., Brandner R., 2006. Kinematics of the Inntal shear zone-sub-Tauern ramp fault system and the interpretation of the TRANSALP seismic section, Eastern Alps, Austria. Tectonophysics 414, 241–258. https://doi.org/10.1016/j.tecto.2005.10.017

Pomella H., Costantini D., Aichholzer P., Reiser M., Schuster R., Tropper P., 2022. Petrological and geochronological investigations on the individual nappes of the Meran-Mauls nappe stack (Austroalpine unit/South Tyrol, Italy). Austrian Journal of Earth Sciences 115, 15–40. https://doi.org/10.17738/ajes.2022.0002

Pomella H., Flöss D., Speckbacher R., Tropper P., Fügenschuh B., 2016. The western end of the Eoalpine High-Pressure Belt (Texel Unit, South Tyrol/Italy). Terra Nova 28, 60–69. https://doi.org/10.1111/ter.12191

Powell R., Holland T.J.B., 2008. On thermobarometry. Journal of Metamorphic Geology 26, 155–179. https://doi.org/10.1111/j.1525-1314.2007.00756.x

Purtscheller F., 1967. Zur Gliederung der Metamorphose im Bereich des Ötztaler-Stubaier Altkristallins. Joanneum - Mineralogisches Mitteilungsblatt (Graz), 1967, 80–85.

Purtscheller F., Rammlmair D., 1982. Alpine metamorphism of diabase dikes in the Ötztal-Stubai Metamorphic Complex. Tschermaks mineralogische und petrographische Mitteilungen 29, 205–221. https://doi.org/10.1007/BF01084643

Rammlmair D., 1980. Petrographie der Diabase der Ötztaler-Stubaier Masse. Diss. Univ. Innsbruck.

Schmid S.M., Froitzheim N., 1993. Oblique slip and block rotation along the Engadine line. Eclogae Geologicae Helvetiae 86, 569–593. https://doi.org/10.5169/seals-167253

Schmid S.M., Haas R., 1989. Transition from near-surface thrusting to Intrabasement Decollement, Schlinig Thrust, eastern Alps. Tectonics 8, 697–718. https://doi.org/10.1029/TC008i004p00697

Schmid S.M., Fügenschuh B., Kissling E., Schuster R., 2004. Tectonic map and overall architecture of the Alpine orogen. Eclogae Geologicae Helvetiae 97, 93–117. https://doi.org/10.1007/s00015-004-1113-x

Schorn S., Stüwe K., 2016. The Plankogel detachment of the Eastern Alps: petrological evidence for an orogen-scale extraction fault. Journal of Metamorphic Geology, 34, 147–166. https://doi.org/10.1111/jmg.12176

Schumacher J.C., 2007. Metamorphic amphiboles: composition and coexistence. Reviews in Mineralogy and Geochemistry 67, 359–416. https://doi.org/10.2138/rmg.2007.67.10

Selverstone J., 1988. Evidence for east-west crustal extension in the eastern Alps: implications for the unroofing history of the Tauern Window. Tectonics 7, 87–105. https://doi.org/10.1029/TC007i001p00087

Sölva H., Thöni M., Grasemann B., Linner M., 2001. Emplacement de roches de haute pression eo-alpines dans le complexe austroalpin de l'Otztal (massif de Texel, Italie du nord). Geodinamica Acta 6, 345–360. https://doi.org/10.1016/S0985-3111(01)01072-5

Sölva H., Grasemann B., Thöni M., Thiede R., Habler G., 2005. The Schneeberg normal fault zone: normal faulting associated with Cretaceous SE-directed extrusion in the Eastern Alps (Italy/Austria). Tectonophysics 401, 143–166. https://doi.org/10.1016/j.tecto.2005.02.005

Spalla M.I., 1993. Microstructural control on the PT path construction in metapelites from the Austroalpine crust (Texel Gruppe, Eastern Alps). Schweizerische Mineralogische und Petrographische Mitteilungen 73, 259–275. https://doi.org/10.5169/seals-55573

Stumpf S., Skrzypek E., Stüwe K., 2024. Dating prograde metamorphism: U-Pb geochronology of allanite and REE-rich epidote in the Eastern Alps. Contributions to Mineralogy and Petrology, 179, 63. https://doi.org/10.1007/s00410-024-02130-3

Tenczer V., Stüwe K., 2003. The metamorphic field gradient in the eclogite type locality, Koralpe region, Eastern Alps. Journal of Metamorphic Geology, 21, 377–393. https://doi.org/10.1046/j.1525-1314.2003.00448.x

Tessadri R., 1981. Zur Metamorphose am Ostende des Schneeberger Zuges (Sterzing-Südtirol). Diss. Univ. Innsbruck.

Thöni M., 1980. Distribution of pre-Alpine and Alpine metamorphism of the southern Ötztal Mass and the Scarl Unit, based on K/Ar age determinations. Mitt. österr. geol. Ges. 71, 139–165.

Thöni M., 1999. A review of geochronological data from the Eastern Alps. Swiss Journal of Geosciences Supplement 79, 209–230. https://doi.org/10.5169/seals-60206

Thöni M., 2006. Dating eclogite-facies metamorphism in the Eastern Alps–approaches, results, interpretations: a review. Mineralogy and Petrology 88, 123–148. https://doi.org/10.1007/s00710-006-0153-5

Thöny W.F., Tropper P., Schennach F., Krenn E., Finger F., Kaindl R., Bernhard F., Hoinkes G., 2008. The metamorphic evolution of migmatites from the Ötztal Complex (Tyrol, Austria) and constraints on the timing of the pre-Variscan high-T event in the Eastern Alps. Swiss Journal of Geosciences 101, 111–126. https://doi.org/10.1007/s00015-008-1290-0

Tribus M., 2008. Petrologische und thermobarometrische Untersuchungen des amphibolit/eklogitfaziellen eo-Alpinen Events in den Metabasiten des Texel Komplexes. Diploma thesis, Univ. Innsbruck.

Tribus M., Tropper P., Habler G., 2008. Multi-equilibrium thermobarometry of eclogites from the Texel Complex South-Tyrol, Italy. Journal of Alpine Geology 49, 223–224.

Tropper P., Hoinkes G., 1996. Geothermobarometrie in Al2SiO5 führenden Metapeliten des westlichen Ötztal Kristallins. Mineralogy and Petrology 58, 145–170. https://doi.org/10.1007/BF01172094

Tropper P., Recheis A., 2003. Garnet zoning as a window into the metamorphic evolution of a crystalline complex: the northern and central Austroalpine Ötztal-Complex as a polymorphic example. Mitteilungen der Österreichischen Geologischen Gesellschaft 94, 27–53.

Tropper P., Tribus M., Habler G., 2023. The metabasites from the Texel Unit (Austroalpine Unit stack): markers of Cretaceous intracontinental subduction and subsequent collision. Austrian Journal of Earth Scien ces 116, 165–179. https://doi.org/10.17738/ajes.2023.0010

Whitney D.L., Evans B.W., 2010. Abbreviations for names of rock-forming minerals. American mineralogist 95, 185–187. https://doi.org/10.2138/am.2010.3371

Zanchetta S., Poli S., Rubatto D., Zanchi A., Bove G.M., 2013. Evidence for deep subduction of Austroalpine crust (Texel Complex, NE Italy). Rendiconti Lincei 24, 163–176. https://doi.org/10.1007/s12210-013-0239-z

Zanon R., 2010. Strukturgeologische Aufnahme im nördlichen Ötztal-Stubai Komplex bei Flaurling: mit besonderer Berücksichtigung der Deckengrenze ÖSK-Phyllitzone. Diploma thesis, Univ. Innsbruck.

http://geokatalog.buergernetz.bz.it. Online platform of geodata, Autonomous Province of Bozen/Bolzano (Italy).

Received: 16.10.2025
Accepted: 7.2.2025
Editorial Handling: Kurt Stüwe